

Learning Feature Inversion for Multi-class Anomaly Detection under General-purpose COCO-AD Benchmark

Jiangning Zhang^{1,2} · Chengjie Wang² · Xiangtai Li³ · Guanzhong Tian¹ ·
Zhucun Xue¹ · Yong Liu¹ · Guansong Pang⁴ · Dacheng Tao³

Received: date / Accepted: date

Abstract Anomaly detection (AD) is often focused on detecting anomaly areas for industrial quality inspection and medical lesion examination. However, due to the specific scenario targets, the data scale for AD is relatively small, and evaluation metrics are still deficient compared to classic vision tasks, such as object detection and semantic segmentation. To fill these gaps, this work first constructs a large-scale and general-purpose COCO-AD dataset by extending COCO to the AD field. This enables fair evaluation and sustainable development for different methods on this challenging benchmark. Moreover, current metrics such as AU-ROC have nearly reached saturation on simple datasets, which prevents a comprehensive evaluation of different methods. Inspired by the metrics in the segmentation field, we further propose several more practical threshold-dependent AD-specific metrics, *i.e.*, $mF_{1.8}^2$, $mAcc_{.8}^2$, $mIoU_{.8}^2$, and $mIoU_{max}$. Motivated by GAN inversion’s high-quality reconstruction capability, we propose a simple but more powerful InvAD framework to achieve high-quality feature reconstruction. Our method improves the effectiveness of reconstruction-based methods on popular MVTec AD, VisA, and our newly proposed COCO-AD datasets under a multi-class unsupervised setting, where only a single detection model is trained to detect anomalies from different classes. Extensive ablation experiments have demonstrated the effectiveness of each component of our InvAD. Full codes and models are available at <https://github.com/zhangjn/ader>.

Jiangning Zhang (186368@zju.edu.cn)

✉ Yong Liu (yongliu@iipc.zju.edu.cn)

¹ Zhejiang University, Hangzhou, China.

² YouTu Lab, Tencent, Shanghai, China.

³ Nanyang Technological University, Singapore.

⁴ Singapore Management University, Singapore.

1 Introduction

Visual unsupervised anomaly detection only requires training on normal images to achieve classification/segmentation of abnormal images, *a.k.a.*, detection/localization by works [9, 29]. This technique is receiving increasing attention due to its low-cost unsupervised training approach and significant practical implications, *e.g.*, industrial defect detection and medical lesion detection. Current methods [12, 26, 32] generally follow a single-class setting in which each class requires a separate model, significantly increasing the training and memory costs. Recently, UniAD [52] proposes a challenging yet more practical multi-class setting (detailed in Sec. 2), in which we need to handle multiple anomaly classes using just a single model. This paper investigates this challenging task, delving into the three key elements: dataset, metrics, and methods.

By analyzing current representative AD datasets [4, 57, 65], we observe that they are domain-specific with the simple background scene, and the number of images and categories is much smaller compared with related semantic segmentation dataset like COCO [27]. Taking the popular MVTec AD [4] dataset as an example (Fig. 1-Left), it only contains 15 industrial products in 2 types with 3,629 normal images for training and 467/1,258 normal/anomaly images for testing (5,354 images in total). There is no AD dataset with a status equivalent to ImageNet-1K [13] in the classification field or COCO [27] in detection/segmentation fields. Therefore, starting from essential one-class classification ability of visual AD task and considering the cost of constructing a dataset, this paper proposes an AD-specific, general-purpose, and large-scale COCO-AD based on recycling COCO 2017 [27] to evaluate different algorithms under a more challenging and fair benchmark (Sec. 3.1). For

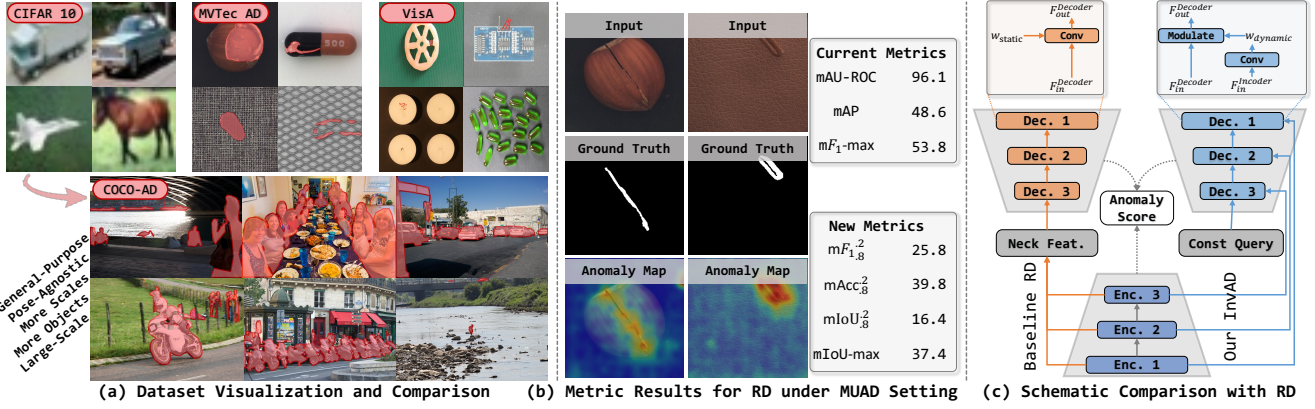


Fig. 1: **Left:** Comparison among representative anomaly detection datasets and our proposed general-purpose COCO-AD. **Middle:** Example visualization of RD on MVTec AD dataset [4]. The excessively high current metrics (especially mAU-ROC) does not align with the visualization results, while our segmentation-inspired metrics provide more objective outcomes. **Right:** Schematic comparison between RD [12] and our *feature inversion* framework.

example, if “car” is considered as an normal class, it will not appear in the training set but need to be detected in the test phase. This can assist us in detecting non-specific new semantic regions for practical application.

In addition, we analyze the current evaluation metrics, *i.e.*, image-/pixel-level AU-ROC [61], AP [55], and F_1 -max [65], as well as AU-PRO [5]. Since these metrics are not primitively designed for the AD field, they have certain flaws in evaluation (Sec. 3). *E.g.*, RD [12] reaches very high threshold-independent sorting AU-ROC score on MVTec AD (Fig. 1-Middle) and it has nearly reached saturation under the single-class setting, meaning that AU-ROC cannot effectively distinguish the merits of different algorithms. Appropriate AD evaluation criteria are essential for judging the merits of different methods. Therefore, based on practical application perspectives, we design four practical and threshold-dependent AD metrics by observing anomaly map distribution and borrowing from semantic segmentation field (Sec. 3.2).

After that, we categorize current AD methods into three types. 1) **Augmentation-based methods** [25, 32, 46, 55, 56] design various anomaly synthesis methods to assist model training. However, these approaches increase training complexity and may lead to dataset bias, resulting in weaker generalization ability. 2) **Embedding-based methods** [5, 11, 14, 37, 60] generally require feature comparison in high-dimensional latent space, which is computationally expensive and susceptible to noise data. 3) **Reconstruction-based methods** [2, 7, 12, 26, 52, 61] follow the naive auto-encoder architecture, which can locate abnormal areas through reconstruction error without the need for carefully designed complex modules. For instance, RD [12] achieves impressive results using only cosine distance [33] as the reconstruction loss. This paper explores this type of technique in-depth. Essentially,

modeling under the multi-class setting is particularly challenging, while the effectiveness of reconstruction-based methods largely benefits from their reconstruction capabilities [29]. Inspired by the high-quality image reconstruction ability of **GAN inversion** [50], we extend this concept to feature-level reconstruction by borrowing the **StyleGAN** [21] design, expecting locating the abnormal area through high-precision reconstruction error. As shown in Fig. 1-Right, we introduce a dynamic modulation mechanism for high-precision feature reconstruction from constant query, which is significantly different from RD [12] using static convolution to reconstruct target features from neck features. **Benefit from input-aware modeling**, the proposed InvAD achieves obvious superiority over different types of state-of-the-art (SoTA) methods (see Fig. 2-Right and Sec. 5.2 for more details).

In summary, this research elevates the multi-class AD task to a more practical level from the perspectives of the dataset, evaluation metrics, and methods. Our contributions are four-fold:

- 1) For dataset, in response to the issues in current mainstream visual AD datasets, we extend the COCO dataset to general visual AD scenarios and propose a highly challenging benchmark to evaluate different methods fairly. We reproduce different types of recent methods on this benchmark (Sec. 3.1).
- 2) For metric, considering the limitations of current AD metrics, **we propose four additional pixel-level metrics** that are more in line with actual application scenarios and suggest reporting five average metrics to holistically evaluate the merits of different methods (Sec. 3.2).
- 3) For method, drawing on the concept of GAN inversion, we design a novel InvAD and propose an Spatial Style Modulation (SSM) module to ensure input-independent and high-quality reconstruction. Without

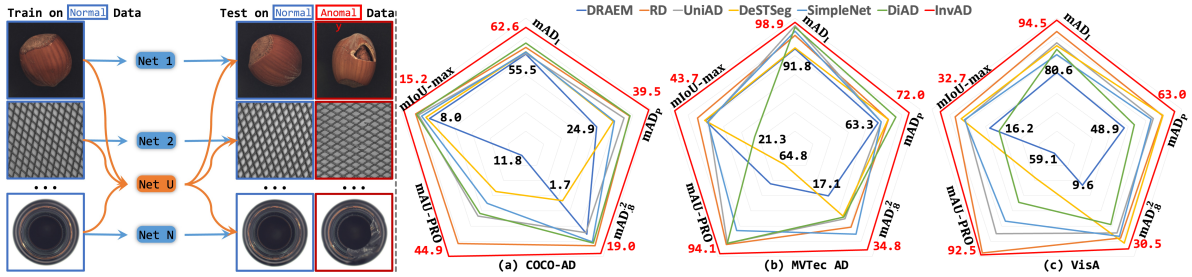


Fig. 2: **Left:** Schematic AD task. **Right:** Performance comparison among our InvAD and SoTA methods.

bells and whistles, InvAD achieves very competitive results by using only pixel-level MSE constraint (Sec. 4). **4)** Our method shows a significant improvement over SoTA methods on the proposed challenging COCO-AD dataset. We also conduct experiments on other representative datasets, achieving obvious new heights in multi-class AD task (Sec. 5).

2 Related Work

Visual Anomaly Detection follows an unsupervised setting, assuming the model only sees normal data during training and must distinguish between normal and anomaly data during testing. This paper categorizes current methods into three main taxonomies. **1) Augmentation-based** methods typically involve synthesizing anomalous regions on normal images [10, 18, 25, 46, 55, 56] or adding anomalous information on normal features to construct pseudo-supervisory signals for training [32, 52]. Recently, multi-class UniAD [52] introduced a feature jittering strategy. The above methods achieve good results, and the augmentation parts can generally be embedded as plug-and-play modules into other approaches to improve performance further, but they require carefully designed model architectures and significantly increase model complexity. **2) Embedding-based** methods generally use a pre-trained model [13] to extract rich feature representations and then distinguish between normal and abnormal features in a compact feature space. They can generally be divided into three categories [29]: *i*) distribution-map based [24, 36, 49, 63], *ii*) teacher-student based [5, 8, 44, 47, 60], and *iii*) memory-bank based [20, 30, 37, 38, 43] methods. **3) Reconstruction-based** methods typically include an encoder that maps the input to a high-dimensional hidden space and a decoder that restores the original data, with anomalies located based on data differences during testing. They can be divided into two categories based on the reconstructed data type. *i*) Image-level methods [2, 16, 26, 39, 51, 55, 61] reconstruct images in the original RGB space, which can be seen as an auto-encoder structure to some extent. *ii*) Feature-level methods [15, 53, 57] further reconstruct input at a more expressive feature level. UniAD [52] in-

troduces a layer-wise query decoder and feature jittering to better model feature-level distribution, while recent works [7, 12, 41] introduce a reverse distillation paradigm to reconstruct multi-resolution features, further enhancing the model’s sensitivity to the different granularity of features. Considering effectiveness and ease-of-use of reconstruction-based methods, this paper introduces the feature inversion concept to improve the technique, hoping to enhance the performance by improving the reconstruction ability.

Multi-class Anomaly Detection Most current methods [12, 37, 55] predominantly focus on single-class unsupervised anomaly detection (SUAD). As illustrated in Fig. 2-Left (marked in blue), each class of objects requires a separate model for training and testing, leading to increased costs in training and deployment. Comparatively, we investigate the more challenging task of multi-class unsupervised anomaly detection (MUAD) that is widely employed by recent works [16, 52, 57]. As shown in the orange indicator of Fig. 2, this more practical setting only requires one unified model to complete testing and deployment for multiple classes, and this paper focuses on this challenging setting.

Challenging AD Datasets are extremely important for developing the AD field. Early methods [29] experiment with CIFAR10 dataset [23] under the semantic setting. Since MVTec AD dataset [4] is proposed, the conventional sensory setting has started to get on track. It gradually enters the field of view of researchers and practitioners, followed by a series of datasets being proposed thrillingly. *E.g.*, KolektorSDD [40], MTD [19], BTAD [35], MVTec LOCO AD [3], PAD [62], and the recently popular VisA [65]. Recently, some 3D-related AD datasets have further been proposed, such as MVTec 3D AD [6] and Real3D [28]. This paper focuses on unsupervised AD tasks in 2D scenarios. However, most current datasets are designed for manufacturing or specific application scenarios. In contrast, the category number and scale of datasets are relatively small, *i.e.*, there is no AD dataset equivalent to the ImageNet-1K [13] in the classification field or the COCO dataset [27] in the detection/segmentation fields. Therefore, we extend the well-known COCO to a general-purpose and large-scale

Table 1: Comparison of current popular AD datasets on different attributes. ✓: Satisfied. ✗: Unsatisfied.

Information-level	Dataset	Classes		Image Number			Split	Multi-object/defect per image	General Purpose	Pose-Agnostic	Scale-Agnostic	Semantic-/Appearance-Agnostic	Complex Background
		Train	Test	Train	Normal	Anomaly							
Semantic	CIFAR10	5	5+5	25,000	5,000	5,000	4	✗	✗	✓	✓	✓	✗
Sensory	MVTec AD	15	15	3,629	467	1,258	1	✗	✗	✗	✗	✗	✗
	MVTec AD-3D	10	10	2,950	249	948	1	✗	✗	✗	✗	✗	✗
	VisA	12	12	8,659	962	1,200	1	✗	✗	✗	✗	✗	✗
Semantic + Sensory	COCO-AD	1 + 60	1 + 60+20	30,438 65,133 79,083	1,291 2,785 3,328	3,661 2,167 1,624	4	✓	✓	✓	✓	✓	✓
				77,580	3,253	1,699							

AD dataset, termed COCO-AD, to evaluate different algorithms. We also conduct a detailed discussion with popular MVTec AD and VisA datasets under the multi-class unsupervised AD setting in Sec. 3.1.

Reasonable Evaluation Metrics are essential for judging the merits of different methods. Current AD metrics include AU-ROC [61], AP [55], F_1 -max [65], and AU-PRO [5], where the first three indicators will simultaneously report both image-/pixel-level results. Current methods generally use part of these metrics for comparison, but this is unreasonable since these metrics are not perfectly fitted, let alone use less (*c.f.*, Sec. 3.2). *E.g.*, AU-ROC has almost reached saturation, and threshold-independent sorting metrics are difficult to guide practical applications. We argue that the current AD evaluation manner is insufficient, so we propose several more practical threshold-dependent metrics for a comprehensive comparison.

GAN Inversion aims to utilize a pre-trained generator to find the latent space encoding corresponding to a given image [50], thereby enabling the faithful reconstruction of the input image via the inverted code by the generator. Current methods can be principally divided into **optimization-based** and **learning-based**. The former directly optimizes the latent vector to minimize the reconstruction error between input/output images [1, 22]. The latter trains a learnable encoder to implement the transformation from real images to hidden features [42, 48, 64] (*c.f.*, Fig. 4-Left). This method trades a certain level of editing accuracy for a one-forward process, and due to its faster speed, this approach has received more attention from researchers. Inspired by the latter, we extend this concept to high-quality feature reconstruction to determine anomalous regions. In other words, while GAN inversion plays an essential role in bridging real and fake image domains, our approach bridges real and fake feature domains.

3 COCO-AD Dataset and Related Metrics

3.1 General-purpose COCO-AD Benchmark

Anomaly detection datasets can be divided into two categories: semantic and sensory settings [29]. The former is typically represented by the CIFAR10 classification

dataset [23]. As shown in the first row in Table 1, this semantic setting treats a subset of 5 categories as normal and the rest as anomalies. It can be seen as a special case of novelty detection, differing from the general definition of visual AD. The popular sensory MVTec AD dataset [4] represents the latter, commonly used in manufacturing scenarios to capture and detect unknown types of sensory defects, such as broken, scratched, or holed items. Due to its high practical value, subsequent research has primarily adopted this setting, and a series of related datasets have been proposed, such as recent VisA [65] and Real-IAD [45].

Motivation. We find that current datasets are mostly targeted at manufacturing or specific application scenarios, and the category number and scale are relatively small. In addition, there is no general-purpose AD dataset with a status similar to the ImageNet-1K [13] in the classification field or the COCO [27] dataset in the detection and segmentation fields, which could result in insufficient method evaluation for practical use and limit the healthy development in the AD field. Therefore, it is particularly necessary to construct a large-scale and general-purpose challenging AD dataset.

Adapting COCO to AD field. Starting from essential one-class classification ability of visual AD task, we summarize the characteristics that an anomaly detection dataset for general scenarios should include: 1) large-scale data volume, 2) category diversity, 3) scenario diversity, 4) semantic texture diversity, and 5) non-fixed pose shooting. Specifically, we ponder the feasibility of current detection and segmentation datasets for AD tasks and intriguingly find that general scenario datasets with semantic segmentation annotations naturally fit AD tasks. Considering the cost and effectiveness of data acquisition, we propose a general-purpose COCO-AD benchmark based on COCO 2017 [27] to evaluate different AD methods fairly, which includes a variety of semantic categories and challenging sensory differences within each category. Specifically, we take 20 categories in sequence as anomaly classes and the remaining 60 categories plus one background class as normal classes, constructing four splits without category overlapping for benchmarking. As a result, each split supports an MUAD setting of 80 classes natively. As shown in the

Table 2: Comparison of various AD metrics. ‘m’ prefix: averaged results. Red metrics are recommended.

			Highlight
mAU ₁	Fineness-level	Metric	
	Image-level (Classification)	mAU-ROC	Area Under the ROC curve (TPR vs. FPR) to evaluate binary classification models Threshold-independent sorting metric
		mAP	Average Precision (<i>a.k.a.</i> , AU-PR) that is Area Under the PR curve (Precision vs. Recall) Threshold-independent sorting metric
mAU ₂ , mAU _P	Region-level	mF ₁ -max	F ₁ -score at optimal threshold Threshold-dependent metric Against potential data imbalance
	Pixel-level (Segmentation)	mAU-PRO	Area Under the Per-Region-Overlap (PRO vs. FPR) Weighting regions of different size equally Threshold-independent sorting metric
		mAU-ROC	Same as above Large predicted correct areas can compensate small incorrect areas
Proposed		mAP	Same as above More appropriate for highly imbalanced classes
		mF ₁ -max	Same as above Advantageous deployment-time
		mF ₁ . ² _{.8}	Average F ₁ -score with thresholds ranging from 0.2 to 0.8 Threshold-dependent metric
		mAcc. ² _{.8}	Average Accuracy with thresholds ranging from 0.2 to 0.8 Threshold-dependent metric
		mIoU. ² _{.8}	Average Intersection over Union with thresholds ranging from 0.2 to 0.8 Threshold-dependent metric
		mIoU-max	Intersection over Union Intuitively reflect the accuracy and overlap Threshold-dependent metric

Table 3: Results of the Pearson correlation coefficient between each pair of datasets based on the fundamental seven indicators and additional four new metrics.

Dataset	Method	seven metrics			w/ new metrics			
		MVTec AD [4]	VisA [65]	COCO-AD	RD [12]	UniAD [52]	SimpleNet [32]	DiAD [16]
	MVTec AD [4]	✓	✓	✗	✓	✓	✗	✓
	VisA [65]	✓	✗	✓	✓	✗	✓	✓
	COCO-AD	✗	✓	✓	✓	✓	✓	✓
	RD [12]	0.994	0.933	0.924	0.987	0.924	0.953	
	UniAD [52]	0.988	0.893	0.890	0.982	0.925	0.945	
	SimpleNet [32]	0.984	0.903	0.872	0.987	0.920	0.926	
	DiAD [16]	0.989	0.878	0.912	0.965	0.893	0.952	
	InvAD	0.996	0.931	0.930	0.990	0.929	0.954	

right five columns of Table 1, its intuitive attribute comparison with current popular datasets indicates the challenges of COCO-AD from multiple dimensions. Appendix A provides a statistical analysis of the four splits of the COCO-AD dataset across four dimensions to understand its characteristics for the AD task comprehensively. Furthermore, intuitive visualizations are shown in Fig. 1-Left and Appendix C. Notably, we provide a construction approach that can be adopted for other related datasets. However, given the challenging nature of the current results (Sec. 5.2) from COCO-AD, there is no need to construct larger datasets.

Feasibility evidence. Table 3-Left shows Pearson correlation coefficient between each pair of datasets based on the current seven image-/pixel-level AU-ROC [61]/AP [55]/F₁-max [65] and region-level AU-PRO [5]. It can be observed that COCO-AD has a high correlation with the other two datasets, indicating its appropriateness for AD tasks. However, its correlation is slightly lower compared to the correlation between industrial MVTec AD and VisA datasets, which suggests its distinguished and general-purpose attributes. Notably, the consistency in the ranking of evaluation results in Sec. 5.2 from different SoTA methods validates the rationality of extending COCO to the AD task. If a method performs better on MVTec AD and VisA, it also tends to perform better on COCO-AD.

3.2 Comprehensive mM_{.8}² and mIoU-max Metrics

As shown in Table 2, we categorize the current evaluation criteria into three types: image-level mAU-ROC [61]/mAP [55]/mF₁-max [65], region-level mAU-PRO [5], and pixel-level mAU-ROC/mAP/,F₁-max.

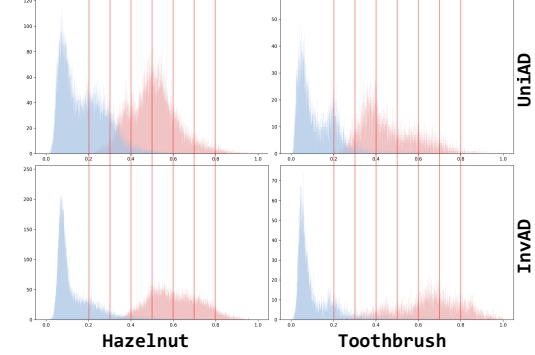


Fig. 3: Anomaly score distribution on object Hazelnut and texture Toothbrush. Our method exhibits less overlap between normal and abnormal values and has a clearer demarcation line. Furthermore, the values tend to be closer to 0 (normal) and 1 (anomaly), respectively.

Limitations of previous metrics. Since above metrics are not specifically designed for the AD domain, they have certain limitations in evaluation. As shown in the ‘Highlight’ column of Table 2, threshold-independent mAU-ROC, mAP, and mAU-PRO disregard the absolute value distribution of prediction probabilities, which may cause accuracy fluctuations due to inappropriate threshold selection in practical applications, while mF₁-max can be affected by potential data imbalance. In addition, above metrics are excessively high (especially mAU-ROC) in current datasets like MVTec AD, but the quantitative results does not align with the visualization results (*c.f.*, Fig. 1-Middle), meaning that they cannot effectively distinguish the merits of different algorithms.

Advancements inspired by segmentation. Considering the higher practical value of pixel-level segmentation and evaluation, we further adapt segmentation metrics to the AD domain, proposing threshold-dependent mF₁.²_{.8}, mAcc.²_{.8}, and mIoU.²_{.8}. 0.2 is a high-confidence threshold often chosen in industry, so we chose a threshold range from 0.2 to 0.8 to align as closely as possible with actual applications. Specifically, these metrics are inspired by the binary classification definition of the AD task. Fig. 3 analyzes the pixel-level anomaly score distribution with SoTA UniAD [52] on object Hazelnut and texture Toothbrush, observing that most anomaly and

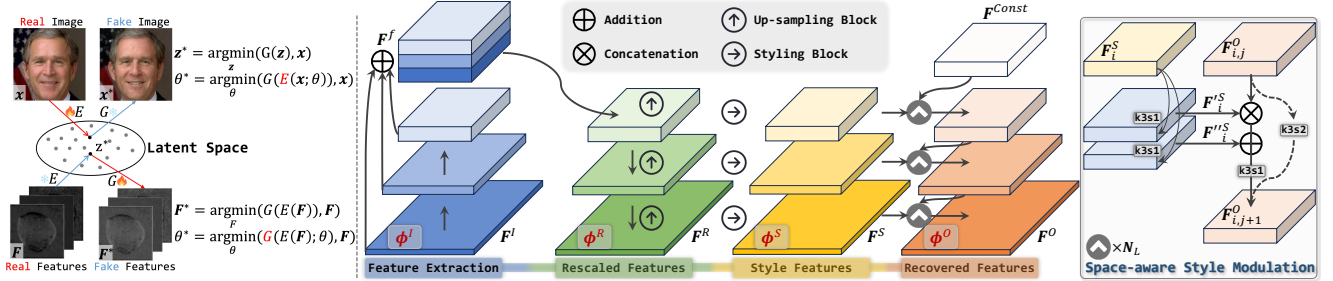


Fig. 4: **Left:** Feature inversion concept inspired by GAN inversion. **Right:** Overview of the proposed InvAD framework that consists of four components in tandem: 1) Multi-scale features \mathbf{F}^I extracted by image encoder ϕ^I is aggregated into low-resolution \mathbf{F}^f to avoid spatial consistency mapping; 2) Re-scaling upsampler ϕ^R obtains re-scaled features \mathbf{F}^R by several Up-sampling Blocks \odot ; 3) An style translator ϕ^S , composed of Styling Block \odot , to obtain style features \mathbf{F}^S as the modulation control signal for the next stage; 4) An feature decoder ϕ^O to recover input features \mathbf{F}^O for loss and anomaly map calculation by cascaded Space-aware Style Modulation modules \circlearrowleft .

normal values fall around 0.5 and exhibit overlap. We argue that a good AD method should output values as close as possible to 0 (normal) or 1 (anomaly) with clear anomaly result judgment and less in intermediate states. Therefore, we calculate the average metric scores for thresholds ranging from 0.2 to 0.8 with a step of 0.1 as the comprehensive score, *i.e.*, $mM_{.8}^2$ ($mM \in mF_1$, $mAcc$, and $mIoU$). Moreover, drawing from the more practical F_1 -max metric design, we introduce the popular $mIoU$ from segmentation into the AD domain, designing the $mIoU$ -max metric to measure the overlap upper limit between different AD method results and ground truth. Considering the dazzling of excessive metrics, we take the average of image-level mAU -ROC/ mAP / mF_1 -max, pixel-level mAU -ROC/ mAP / mF_1 -max, and $M_{.8}^2$ metrics as comprehensive metrics, respectively, marked in red in Table 2. Time consumption (s) for testing various metrics on different datasets by AMD EPYC 7K62 CPU are as follows, and this demonstrates the high efficiency of $mAD_{.8}^2$ and $mIoU$ -max:

Dataset	mAD_I	mAD_P	$mAD_{.8}^2$	mAU -PRO	$mIoU$ -max
MVTec AD	0.003	13.401	0.654	19.555	0.630
VisA	0.005	16.788	0.841	24.195	0.795
COCO-AD	0.005	374.877	20.435	589.95	18.99

We suggest that subsequent works should continue to use comprehensive metrics for evaluation, which has important guiding significance for the practicality. Notably, these new metrics are applicable to single-class AD and they all in the range of [0, 100%].

Rationality explanation. Table 3-Right shows Pearson correlation coefficient between each pair of datasets with additional four new metrics. The correlation between the two industrial datasets slightly decreases, indicating that the new metrics are more challenging for evaluating industry-specific datasets. In addition, these metrics increase when relating more general COCO-AD, demonstrating their universality for practical application.

4 Methodology: InvAD

Motivation. In essence, AD aims at overfitting to the training set with only normal data. Modeling under the multi-class setting is particularly challenging, while the effectiveness of reconstruction-based methods largely benefits from their reconstruction capabilities [29]. As shown in Fig. 4-Left, inspired by the high-quality image reconstruction ability of GAN inversion [50], learning-based GAN inversion fixes the generator G to optimize the best parameters of the encoder E :

$$\theta^* = \operatorname{argmin}_{\theta} (\mathbf{G}(\mathbf{E}(\mathbf{x}; \theta)), \mathbf{x}). \quad (1)$$

Our work extends this concept to feature-level reconstruction, fixing the encoder E to optimize the best parameters of the generator G , and then locating the abnormal area through the positional difference between the original feature \mathbf{F} and the generated feature \mathbf{F}^* :

$$\theta^* = \operatorname{argmin}_{\theta} (\mathbf{G}(\mathbf{E}(\mathbf{F}); \theta), \mathbf{F}). \quad (2)$$

Generally, we follow the powerful StyleGAN [21] generator that is frequently employed in GAN-inversion structures and adapt it to InvAD's structural design.

Overall structure. Inspired by the high-quality reconstruction capability of GAN inversion [50], we design a novel feature inversion AD framework in Fig. 4-Right to perform high-quality feature reconstruction. Specifically, InvAD consists of four components in tandem: 1) Image encoder ϕ^I performs multi-scale feature extraction on input image \mathbf{I} to obtain \mathbf{F}^I , which goes through down-sampling, concatenation, and N_B Bottleneck [17] to get the fusion feature \mathbf{F}^f . Consistent with RD [12], WideResNet-50 [54] is used by default, but combining powerful backbones [31, 58, 59] can potentially improve model performance. 2) Re-scaling upsampler ϕ^R leverages several up-sampling blocks to obtain \mathbf{F}^R , with each

Table 4: **Technical incremental trajectory of InvAD.** Each line modifies the immediately preceding line incrementally. Detailed ablations in Sec. 5.3.

Method	mAD _I	mAD _P	mAD _R ²	mAU-PRO	mIoU-max
Baseline (RD)	95.4	66.2	27.4	91.1	37.3
+ Use Skip AutoEncoder	96.5	69.9	29.8	91.4	41.7
+ Use Rescaled Features ϕ^R	97.7	70.3	34.1	93.4	41.8
+ Use Style Features ϕ^S	98.3	71.0	34.4	93.8	42.5
+ Use SSM (InvAD)	98.9	72.0	34.8	94.1	43.7

block containing an up-sampling convolution followed by N_C convolution modules. 3) Style translator ϕ^S applies two convolution layers to \mathbf{F}_i^R at each resolution to obtain the channel-shrunk style feature \mathbf{F}_i^S . 4) Feature decoder ϕ^O uses \mathbf{F}^S as the space-aware style condition to recover feature \mathbf{F}^O from a constant feature \mathbf{F}^{Const} through several stacked Space-aware Style Modulation (SSM) modules. Each stage simply uses N_L SSMs.

SSM module. To increase dynamic modeling capabilities, we introduce a modulation mechanism for high-precision feature reconstruction from constant query, which is significantly different from RD [12] using static convolution to reconstruct target features from neck features. Specific structure is shown in Fig. 4-Right: \mathbf{F}_i^S passes through two convolution layers with kernel 3 and stride 1 (k3s1) to obtain $\mathbf{F}_i'^S$ and $\mathbf{F}_i''^S$, which serves as the control signal for $SSM_{i,j}$:

$$\mathbf{F}_{i,j+1}^O = (\mathbf{F}_i'^S \otimes (\mathbf{F}_{i,j}^O - \mu(\mathbf{F}_{i,j}^O)) / \sigma(\mathbf{F}_{i,j}^O)) \oplus \mathbf{F}_i''^S, \quad (3)$$

where i represents the stage, and $j \in [1, N_L]$ represents the j -th SSM module under the i -th resolution. $\mu(\cdot)$ and $\sigma(\cdot)$ compute the mean and variance of a feature. Notably, this module also supports up-sampling operations labeled as k3s2 with kernel 3 and stride 2.

Implementation details. The channel numbers N_R and N_S of \mathbf{F}^R and \mathbf{F}^S at each stage are set to 64 and 16 by default, ensuring a relatively low increase in computational load. Cosine distance between \mathbf{F}^I and \mathbf{F}^O is viewed as anomaly map during inference [12]. Overall, the entire InvAD only contains convolution operations and requires only MSE reconstruction constraints, making it simple, efficient, and effective. We provide InvAD with Wide-ResNet-50 [54] as the default encoder model, and also offer a lighter InvAD-lite with ResNet-34 [17].

InvAD Summary. Starting from the basic RD [12], we gradually fuse each proposed component to build our InvAD step-by-step. Table 4 reveals the effectiveness of each design, and we obtain the powerful InvAD model when using all components.

5 Experiments

5.1 Setup for Multi-class Unsupervised AD

Datasets. This paper investigates the problem of anomaly classification and segmentation under a multi-

class setting. In addition to evaluating the potential of different methods on the newly proposed general-purpose large-scale COCO-AD benchmark, we also conduct comparative experiments on MVTec AD [4] and VisA [65]. Considering computational costs, all ablation and analysis experiments are conducted on the popular MVTec AD by default. We also provide results on the MVTec3D [6], as well as the recently proposed Uni-Medical [57], and Real-IAD [45] datasets.

Metrics. This paper suggests using image-level AU-ROC [61]/AP [55]/ F_1 -max [65], region-level AU-PRO [5], and pixel-level AU-ROC/AP/ F_1 -max to evaluate the results of different methods comprehensively. Furthermore, we evaluate the newly proposed metrics (Sec. 3.2) and standardized several average AD metrics for comprehensive comparison.

Comparison Methods. We reproduce mainstream models under the MUAD setting for fair comparison: augmentation-based DRÆM [55], embedding-based SimpleNet [32]/DeSTSeg [60], and reconstruction-based RD [12]/UniAD [52]/DiAD [16]. Note that all methods are re-trained under 256×256 resolution.

Training Details. InvAD is trained under 256×256 resolution with only MSE reconstruction loss, without any extra datasets and training tricks/augmentations for all experiments. AdamW optimizer [34] is used with an initial learning rate of $1e^{-4}$, a weight decay of $1e^{-4}$, and a batch size of 32. Our model is trained for 300 epochs by a single V100 GPU on MVTec AD and VisA datasets, and the learning rate drops by 0.1 after 80 percent epochs. For the COCO-AD dataset, all methods are trained fairly for 100 epochs.

5.2 Results on COCO-AD, MVTec AD, and VisA

Quantitative results. Table 5 presents a quantitative comparison of our InvAD with SoTA methods on the COCO-AD (complex general scenarios), MVTec AD (specific industrial scenarios), and VisA (small defects) datasets regarding comprehensive metrics. Overall, our InvAD consistently achieves significantly higher results on all metrics, validating the effectiveness of the proposed feature inversion structure. Additionally, we discover several interesting findings through the results: *i*) Although the image-level metrics of MVTec are nearly saturated, they still hold research value for the region-/pixel-level results, especially on the proposed more practical mIoU-max. *ii*) As the first general-purpose dataset, the highly challenging COCO-AD has lower results on all metrics, serving as a standard benchmark to promote the continuous development of AD algorithms. *iii*) Different types of existing algorithms tend to a certain dataset, but the reconstruction-based RD performs relatively stable.

Table 5: Different fine-grained multi-class anomaly classification and segmentation results with SoTAs on representative AD datasets. *: reproduce MUAD results. Prefix ‘m’ stands for averaged metric results for all categories. Metrics marked in red are recommended. **Bold** and underline represent optimal and sub-optimal results, respectively. More results on MVTec 3D AD [6], Uni-Medical [57], and Real-IAD [45] in Appendix D. Abundant results for each category are in Appendix E F G H I J for the restricted space.

	Fineness-level	Metric	DR/EM* [55]	RD* [12]	UniAD [†] [52]	DeSTSeg* [60]	SimpleNet* [32]	DiAD [16]	InvAD-lite	InvAD
COCO-AD	Image-level (Classification)	mAU-ROC	55.1	58.4	56.2	56.2	57.1	59.0	<u>64.7</u>	65.9
		mAP	48.9	51.1	49.0	50.3	49.4	53.0	<u>56.7</u>	57.8
		mF ₁ -max	62.5	62.3	61.7	61.9	61.7	63.2	<u>63.5</u>	64.1
	Region-level	<u>mAU-PRO</u>	11.8	40.7	31.7	23.6	27.5	30.8	38.2	<u>44.9</u>
	Pixel-level (Segmentation)	mAU-ROC	51.8	67.4	65.4	60.9	59.5	68.1	<u>70.6</u>	73.3
		mAP	8.4	14.3	12.9	11.3	12.2	20.5	18.4	<u>19.7</u>
		mF ₁ -max	14.5	20.6	19.4	16.3	17.9	14.2	23.4	<u>25.4</u>
	Proposed	mF ₁ , _s	7.9	9.9	6.6	2.4	8.5	9.6	<u>11.2</u>	12.4
		mAcc, _s	24.4	33.8	26.4	1.5	32.3	31.1	<u>34.2</u>	37.5
		mIoU, _s	5.6	5.5	3.7	1.2	4.7	6.1	<u>6.4</u>	7.1
		<u>mIoU-max</u>	8.0	11.9	11.1	9.0	10.2	11.6	<u>13.8</u>	15.2
MVTec AD [4]	Averaged Metrics	mAD _I	55.5	57.3	55.6	56.1	56.0	58.4	<u>61.6</u>	62.6
		mAD _P	24.9	34.1	32.6	29.5	29.9	34.2	<u>37.4</u>	39.5
		mAD _S	12.6	16.4	12.2	1.7	15.2	15.6	<u>17.3</u>	19.0
	Image-level (Classification)	mAU-ROC	88.8	94.6	97.5	89.2	95.3	97.2	98.2	98.9
		mAP	94.7	96.5	99.1	95.5	98.4	99.0	99.2	99.6
		mF ₁ -max	92.0	95.2	97.3	91.6	95.8	96.5	97.2	98.1
	Region-level	<u>mAU-PRO</u>	71.1	91.1	90.7	64.8	86.5	90.7	<u>92.7</u>	94.1
	Pixel-level (Segmentation)	mAU-ROC	88.6	96.1	97.0	93.1	96.9	96.8	<u>97.4</u>	98.2
		mAP	52.6	48.6	45.1	54.3	45.9	52.6	<u>55.0</u>	57.6
		mF ₁ -max	48.6	53.8	50.3	50.9	49.7	55.5	<u>58.1</u>	60.1
VisA [65]	Proposed	mF ₁ , _s	21.8	25.8	22.4	29.7	25.3	19.5	<u>22.6</u>	34.6
		mAcc, _s	15.3	39.8	37.5	22.7	47.7	40.7	<u>47.1</u>	46.9
		mIoU, _s	14.2	16.4	13.9	18.8	16.0	12.0	<u>21.3</u>	23.0
		<u>mIoU-max</u>	35.1	37.3	34.2	35.3	34.4	21.3	<u>41.7</u>	43.7
	Averaged Metrics	mAD _I	91.8	95.4	98.0	92.1	96.5	97.6	<u>98.2</u>	98.9
		mAD _P	63.3	66.2	64.1	66.1	64.2	68.3	<u>70.2</u>	72.0
		mAD _S	17.1	27.4	24.6	23.7	29.7	24.1	<u>33.7</u>	34.8
	Image-level (Classification)	mAU-ROC	79.5	92.4	88.8	88.9	87.2	86.8	<u>94.9</u>	95.5
		mAP	82.8	92.4	90.8	89.0	87.0	88.3	<u>95.2</u>	95.8
		mF ₁ -max	79.4	89.6	85.8	85.2	81.7	85.1	<u>90.8</u>	92.1
	Region-level	<u>mAU-PRO</u>	59.1	91.8	85.5	67.4	81.4	75.2	<u>92.5</u>	92.5
COCO-AD	Pixel-level (Segmentation)	mAU-ROC	91.4	98.1	98.3	96.1	96.8	96.0	<u>98.6</u>	98.9
		mAP	24.8	38.0	33.7	39.6	34.7	26.1	<u>40.3</u>	43.1
		mF ₁ -max	30.4	42.6	39.0	43.4	37.8	33.0	<u>44.3</u>	47.0
	Proposed	mF ₁ , _s	12.6	21.2	17.9	27.4	17.5	13.2	<u>25.8</u>	28.0
		mAcc, _s	8.7	46.5	47.1	41.0	50.6	46.2	44.2	45.6
		mIoU, _s	7.4	13.1	10.9	17.3	11.0	8.0	16.1	<u>17.9</u>
		<u>mIoU-max</u>	18.8	28.5	25.7	26.8	25.9	16.2	30.0	<u>32.7</u>
	Averaged Metrics	mAD _I	80.6	91.5	88.5	87.7	85.3	86.7	<u>93.6</u>	94.5
		mAD _P	48.9	59.6	57.0	59.7	56.4	51.7	<u>61.1</u>	63.0
		mAD _S	9.6	26.9	25.3	28.6	26.4	22.5	<u>28.7</u>	30.5

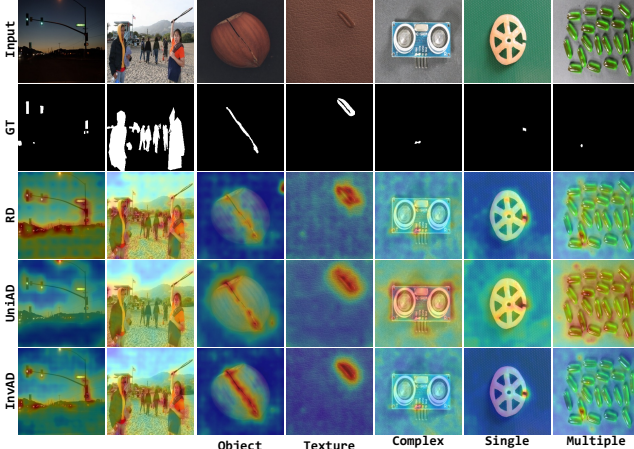


Fig. 5: Visual comparison of anomaly maps for different types of objects on COCO-AD (Left), MVTec AD (Middle), and VisA (Right) datasets. Our InvAD locates more *compact* segmentation results with ground truths while having a smaller response in normal areas.

Qualitative results. Fig. 5 further provides a visual comparison with RD and UniAD on three datasets, selecting one object from each category. Comparatively, InvAD produces *more compact anomaly localization* while having a smaller feature response in normal areas.

5.3 Ablation and Analysis

Sec. 5.2 demonstrates the consistent superiority of our method across three datasets, so all subsequent ablation and analysis experiments are conducted on the MVTec AD dataset by default to save computational resources.

1) Channel numbers of \mathbf{F}^R and \mathbf{F}^S . The upper part of Table 6 shows the results under different configurations of the channel numbers N_R and N_S for \mathbf{F}^R and \mathbf{F}^S . Results indicate that fewer channels are sufficient to achieve satisfactory results. In contrast, an excessive number of channels does not significantly improve the results and instead incurs additional computational costs.

2) Stack numbers of different sub-modules. The lower part of Table 6 shows the impact of different sub-module stacking layers in InvAD on the results, indicating that a configuration of 1/1/2 is sufficient to achieve satisfactory results, and more layers may adversely affect the model performance.

3) Threshold ranges and step sizes of $M_{.8}^2$ metrics. As shown in Table 7, more refined steps will produce more accurate results, but the step of 0.1 is enough while reasonably reducing the evaluation duration. Taking InvAD as an example, more stringent (0.1-0.9) or relaxed (0.4-0.6) threshold ranges would change the results. Considering that 0.2 is a high-confidence threshold often chosen in industry, we chose a threshold in range [0.2,

Table 6: Ablation on architecture: channel numbers of N_R and N_S , and stack numbers N_B , N_C , and N_L .

	N_R	N_S	mAD_I	mAD_P	$mAD_{\frac{2}{8}}$	$mAU-PRO$	$mIoU-max$	
Channel Configure	16	8	98.3	71.1	35.0	94.0	42.7	
Stack Number	16	16	98.5	71.6	35.1	94.1	43.4	
32	8	98.7	71.1	34.8	94.0	42.8		
32	16	98.7	71.5	36.0	94.0	43.0		
64	16	98.9	72.0	34.8	94.1	43.7		
64	32	98.9	71.7	35.6	93.8	43.1		
64	64	98.8	71.7	35.4	94.1	43.3		
128	32	98.8	71.6	34.2	94.2	43.5		
256	64	99.0	71.5	34.0	93.9	42.9		
	N_B	N_C	N_L	mAD_I	mAD_P	$mAD_{\frac{2}{8}}$	$mAU-PRO$	$mIoU-max$
Stack Number	0	0	1	98.5	71.1	33.0	94.0	42.9
0	0	2	98.7	71.5	34.4	93.9	43.0	
0	1	1	98.7	71.6	34.1	94.2	43.4	
1	0	1	98.4	71.2	33.4	94.1	42.9	
1	1	2	98.9	72.0	34.8	94.1	43.7	
1	1	4	98.8	71.7	35.9	94.1	43.3	
1	3	2	98.5	71.9	35.1	94.1	43.8	
3	1	2	98.7	71.8	35.5	94.1	43.3	
3	3	4	98.6	71.0	35.0	93.6	42.7	

Table 7: Ablation experiments for $M_{\frac{2}{8}}$ metrics in terms of start/end thresholds $\theta_{start}/\theta_{end}$ and step.

No.	θ_{start}	θ_{end}	Step	$mF_1\text{-max}_{\frac{2}{8}}$	$mAcc_{\frac{2}{8}}$	$mIoU_{\frac{2}{8}}$	Time (s)
(1)	0.2	0.8	0.01	37.02	46.46	24.73	115.74
(2)	0.2	0.8	0.05	35.93	46.67	23.94	24.84
(3)	0.2	0.8	0.1	34.58	46.91	22.95	13.59
(4)	0.1	0.9	0.1	28.54	47.65	18.76	16.96
(5)	0.2	0.8	0.1	34.58	46.91	22.95	13.59
(6)	0.3	0.7	0.1	40.09	45.79	26.96	9.54
(7)	0.4	0.6	0.1	44.06	44.71	29.78	5.63

Table 8: Ablation for Style Features ϕ^S and SSM.

ϕ^S	SSM	mAD_I	mAD_P	$mAD_{\frac{2}{8}}$	$mAU-PRO$	$mIoU-max$
\times	\times	97.7	70.3	34.1	93.4	41.8
\checkmark	\times	98.3	71.0	34.4	93.8	42.5
\times	\checkmark	98.5	71.3	34.5	93.9	43.0
\checkmark	\checkmark	98.9	72.0	34.8	94.1	43.7

Table 9: Efficiency analysis over SoTAs on MVTec AD.

Method	Train		Test		#Params	FLOPs	FPS
	Memory	Time	Memory	Time			
DREM [55]	32,192M	17.2H	5,990M	31.9s	97.4M	198.0G	54.0
RD [12]	9,008M	4.3H	3,186M	19.0s	80.6M	28.4G	90.6
UniAD [52]	6,164M	12.8H	2,920M	30.4s	24.5M	3.4G	56.8
DeSTSeg [60]	12,698M	5.1H	4,852M	23.1s	35.2M	30.7G	74.7
SimpleNet [32]	6,154M	8.4H	3,123M	35.0s	72.8M	17.7G	49.3
DiAD [16]	21,772M	45.1H	13,502M	1552.5s	1331.0M	451.5G	0.5
InvAD-lite	5,050M	4.2H	2,738M	17.0s	17.2M	9.3G	101.6
InvAD	16,280M	5.4H	9,286M	20.7s	95.6M	45.4G	83.5

0.8] to align with actual applications.

4) Ablations on Style Features ϕ^S and SSM. We remove ϕ^S and replace SSM with cascade concatenation and convolution operations in Table 8. Our InvAD still achieves competitive results even without two modules, and each module contributes performance.

5) Time and memory consumption. We further simplify the hyper-parameter and backbone to ResNet34 to obtain InvAD-lite. While significantly improving efficiency, it achieves *significant* better results over state-of-the-art methods in Table 9. More ablation can be viewed in Appendix B.

6 Conclusion

This work rethinks the multi-class AD task from its three essential elements. Firstly, we construct a large-scale and challenging general-purpose COCO-AD dataset, alleviating the current issues of small dataset size and low scenario complexity. Secondly, we propose four practical threshold-dependent AD-specific metrics for com-

prehensive evaluation. Finally, we propose a powerful InvAD framework to achieve high-quality feature reconstruction, greatly enhancing the effectiveness of reconstruction-based methods on several AD datasets. We hope this work can inspire future research.

References

- Abdal, R., Qin, Y., Wonka, P.: Image2stylegan++: How to edit the embedded images? In: CVPR (2020) [4](#)
- Akcay, S., Atapour-Abarghouei, A., Breckon, T.P.: Ganomaly: Semi-supervised anomaly detection via adversarial training. In: ACCV (2019) [2, 3](#)
- Bergmann, P., Batzner, K., Fauser, M., Sattlegger, D., Steger, C.: Beyond dents and scratches: Logical constraints in unsupervised anomaly detection and localization. IJCV (2022) [3](#)
- Bergmann, P., Fauser, M., Sattlegger, D., Steger, C.: Mvtec ad—a comprehensive real-world dataset for unsupervised anomaly detection. In: CVPR (2019) [1, 2, 3, 4, 5, 7, 8](#)
- Bergmann, P., Fauser, M., Sattlegger, D., Steger, C.: Uninformed students: Student-teacher anomaly detection with discriminative latent embeddings. In: CVPR (2020) [2, 3, 4, 5, 7](#)
- Bergmann, P., Jin, X., Sattlegger, D., Steger, C.: The mvtec 3d-ad dataset for unsupervised 3d anomaly detection and localization. In: VISIGRAPP (2022) [3, 7, 8, 11, 12](#)
- Cao, T., Zhu, J., Pang, G.: Anomaly detection under distribution shift. In: ICCV (2023) [2, 3](#)
- Cao, Y., Wan, Q., Shen, W., Gao, L.: Informative knowledge distillation for image anomaly segmentation. KBS (2022) [3](#)
- Cao, Y., Xu, X., Zhang, J., Cheng, Y., Huang, X., Pang, G., Shen, W.: A survey on visual anomaly detection: Challenge, approach, and prospect. arXiv preprint arXiv:2401.16402 (2024) [1](#)
- Cimpoi, M., Maji, S., Kokkinos, I., Mohamed, S., Vedaldi, A.: Describing textures in the wild. In: CVPR (2014) [3](#)
- Defard, T., Setkov, A., Loesch, A., Audigier, R.: Padim: a patch distribution modeling framework for anomaly detection and localization. In: ICPR (2021) [2](#)
- Deng, H., Li, X.: Anomaly detection via reverse distillation from one-class embedding. In: CVPR (2022) [1, 2, 3, 5, 6, 7, 8, 9, 11, 12, 13, 15, 16, 17, 18, 19, 20, 21, 22, 23](#)
- Deng, J., Dong, W., Socher, R., Li, L.J., Li, K., Fei-Fei, L.: Imagenet: A large-scale hierarchical image database. In: CVPR (2009) [1, 3, 4](#)
- Gudovskiy, D., Ishizaka, S., Kozuka, K.: Cflow-ad: Real-time unsupervised anomaly detection with localization via conditional normalizing flows. In: CACV (2022) [2](#)
- He, H., Bai, Y., Zhang, J., He, Q., Chen, H., Gan, Z., Wang, C., Li, X., Tian, G., Xie, L.: Mambaad: Exploring state space models for multi-class unsupervised anomaly detection. arXiv (2024) [3](#)
- He, H., Zhang, J., Chen, H., Chen, X., Li, Z., Chen, X., Wang, Y., Wang, C., Xie, L.: A diffusion-based framework for multi-class anomaly detection. In: AAAI (2024) [3, 5, 7, 8, 9, 12, 13, 15, 16, 17, 18, 19, 20, 21, 22, 23](#)
- He, K., Zhang, X., Ren, S., Sun, J.: Deep residual learning for image recognition. In: CVPR (2016) [6, 7](#)
- Hu, T., Zhang, J., Yi, R., Du, Y., Chen, X., Liu, L., Wang, Y., Wang, C.: Anomalydiffusion: Few-shot anomaly image generation with diffusion model. In: AAAI (2024) [3](#)

19. Huang, Y., Qiu, C., Yuan, K.: Surface defect saliency of magnetic tile. *The Visual Computer* (2020) [3](#)
20. Jang, J., Hwang, E., Park, S.H.: N-pad: Neighboring pixel-based industrial anomaly detection. In: *CVPR* (2023) [3](#)
21. Karras, T., Laine, S., Aila, T.: A style-based generator architecture for generative adversarial networks. In: *CVPR* (2019) [2](#), [6](#)
22. Karras, T., Laine, S., Aittala, M., Hellsten, J., Lehtinen, J., Aila, T.: Analyzing and improving the image quality of stylegan. In: *CVPR* (2020) [4](#)
23. Krizhevsky, A., Hinton, G., et al.: Learning multiple layers of features from tiny images (2009) [3](#), [4](#)
24. Lei, J., Hu, X., Wang, Y., Liu, D.: Pyramidflow: High-resolution defect contrastive localization using pyramid normalizing flow. In: *CVPR* (2023) [3](#)
25. Li, C.L., Sohn, K., Yoon, J., Pfister, T.: Cutpaste: Self-supervised learning for anomaly detection and localization. In: *CVPR* (2021) [2](#), [3](#)
26. Liang, Y., Zhang, J., Zhao, S., Wu, R., Liu, Y., Pan, S.: Omni-frequency channel-selection representations for unsupervised anomaly detection. *TIP* (2023) [1](#), [2](#), [3](#)
27. Lin, T.Y., Maire, M., Belongie, S., Hays, J., Perona, P., Ramanan, D., Dollár, P., Zitnick, C.L.: Microsoft coco: Common objects in context. In: *ECCV* (2014) [1](#), [3](#), [4](#)
28. Liu, J., Xie, G., Chen, R., Li, X., Wang, J., Liu, Y., Wang, C., Zheng, F.: Real3d-ad: A dataset of point cloud anomaly detection. *NeurIPS* (2024) [3](#)
29. Liu, J., Xie, G., Wang, J., Li, S., Wang, C., Zheng, F., Jin, Y.: Deep industrial image anomaly detection: A survey. *MIR* (2024) [1](#), [2](#), [3](#), [4](#), [6](#)
30. Liu, W., Chang, H., Ma, B., Shan, S., Chen, X.: Diversity-measurable anomaly detection. In: *CVPR* (2023) [3](#)
31. Liu, Z., Lin, Y., Cao, Y., Hu, H., Wei, Y., Zhang, Z., Lin, S., Guo, B.: Swin transformer: Hierarchical vision transformer using shifted windows. In: *ICCV* (2021) [6](#)
32. Liu, Z., Zhou, Y., Xu, Y., Wang, Z.: Simplenet: A simple network for image anomaly detection and localization. In: *CVPR* (2023) [1](#), [2](#), [3](#), [5](#), [7](#), [8](#), [9](#), [12](#), [13](#), [15](#), [16](#), [17](#), [18](#), [19](#), [20](#), [21](#), [22](#), [23](#)
33. Loshchilov, I., Hutter, F.: Stochastic gradient descent with warm restarts. In: *ICLR* (2017) [2](#), [11](#)
34. Loshchilov, I., Hutter, F.: Decoupled weight decay regularization. In: *ICLR* (2019) [7](#)
35. Mishra, P., Verk, R., Fornasier, D., Piciarelli, C., Foresti, G.L.: Vt-adl: A vision transformer network for image anomaly detection and localization. In: *ISIE* (2021) [3](#)
36. Rezende, D., Mohamed, S.: Variational inference with normalizing flows. In: *ICML* (2015) [3](#)
37. Roth, K., Pemula, L., Zepeda, J., Schölkopf, B., Brox, T., Gehler, P.: Towards total recall in industrial anomaly detection. In: *CVPR* (2022) [2](#), [3](#)
38. Salehi, M., Sadjadi, N., Baselizadeh, S., Rohban, M.H., Rabiee, H.R.: Multiresolution knowledge distillation for anomaly detection. In: *CVPR* (2021) [3](#)
39. Song, J., Kong, K., Park, Y.I., Kim, S.G., Kang, S.J.: Anomaly segmentation network using self-supervised learning. In: *AAAIW* (2022) [3](#)
40. Tabernik, D., Šela, S., Skvarč, J., Skočaj, D.: Segmentation-based deep-learning approach for surface-defect detection. *JIM* (2020) [3](#)
41. Tien, T.D., Nguyen, A.T., Tran, N.H., Huy, T.D., Duong, S., Nguyen, C.D.T., Truong, S.Q.: Revisiting reverse distillation for anomaly detection. In: *CVPR* (2023) [3](#)
42. Tov, O., Alaluf, Y., Nitzan, Y., Patashnik, O., Cohen-Or, D.: Designing an encoder for stylegan image manipulation. *ACM TOG* (2021) [4](#)
43. Wan, Q., Gao, L., Li, X., Wen, L.: Industrial image anomaly localization based on gaussian clustering of pre-trained feature. *TIE* (2021) [3](#)
44. Wan, Q., Gao, L., Li, X., Wen, L.: Unsupervised image anomaly detection and segmentation based on pretrained feature mapping. *TII* (2023) [3](#)
45. Wang, C., Zhu, W., Gao, B.B., Gan, Z., Zhang, J., Gu, Z., Qian, S., Chen, M., Ma, L.: Real-iad: A real-world multi-view dataset for benchmarking versatile industrial anomaly detection. In: *CVPR* (2024) [4](#), [7](#), [8](#), [11](#), [12](#)
46. Wang, R., Hoppe, S., Monari, E., Huber, M.F.: Defect transfer gan: diverse defect synthesis for data augmentation. *arXiv preprint arXiv:2302.08366* (2023) [2](#), [3](#)
47. Wang, S., Wu, L., Cui, L., Shen, Y.: Glancing at the patch: Anomaly localization with global and local feature comparison. In: *CVPR* (2021) [3](#)
48. Wang, T., Zhang, Y., Fan, Y., Wang, J., Chen, Q.: High-fidelity gan inversion for image attribute editing. In: *CVPR* (2022) [4](#)
49. Wu, J., Li, X., Xu, S., Yuan, H., Ding, H., Yang, Y., Li, X., Zhang, J., Tong, Y., Jiang, X., Ghanem, B., Tao, D.: Towards open vocabulary learning: A survey. *T-PAMI* (2024) [3](#)
50. Xia, W., Zhang, Y., Yang, Y., Xue, J.H., Zhou, B., Yang, M.H.: Gan inversion: A survey. *TPAMI* (2022) [2](#), [4](#), [6](#)
51. Yan, Y., Wang, D., Zhou, G., Chen, Q.: Unsupervised anomaly segmentation via multilevel image reconstruction and adaptive attention-level transition. *TIM* (2021) [3](#)
52. You, Z., Cui, L., Shen, Y., Yang, K., Lu, X., Zheng, Y., Le, X.: A unified model for multi-class anomaly detection. *NeurIPS* (2022) [1](#), [2](#), [3](#), [5](#), [7](#), [8](#), [9](#), [11](#), [12](#), [13](#), [15](#), [16](#), [17](#), [18](#), [19](#), [20](#), [21](#), [22](#), [23](#)
53. You, Z., Yang, K., Luo, W., Cui, L., Zheng, Y., Le, X.: Adtr: Anomaly detection transformer with feature reconstruction. In: *ICONIP* (2022) [3](#)
54. Zagoruyko, S., Komodakis, N.: Wide residual networks. In: *BMVC* (2016) [6](#), [7](#)
55. Zavrtanik, V., Kristan, M., Skočaj, D.: Draem-a discriminatively trained reconstruction embedding for surface anomaly detection. In: *ICCV* (2021) [2](#), [3](#), [4](#), [5](#), [7](#), [8](#), [9](#), [13](#), [15](#), [16](#), [17](#), [18](#)
56. Zhang, G., Cui, K., Hung, T.Y., Lu, S.: Defect-gan: High-fidelity defect synthesis for automated defect inspection. In: *CACV* (2021) [2](#), [3](#)
57. Zhang, J., Chen, X., Wang, Y., Wang, C., Liu, Y., Li, X., Yang, M.H., Tao, D.: Exploring plain vit reconstruction for multi-class unsupervised anomaly detection. *arXiv preprint arXiv:2312.07495* (2023) [1](#), [3](#), [7](#), [8](#), [11](#), [12](#)
58. Zhang, J., Li, X., Li, J., Liu, L., Xue, Z., Zhang, B., Jiang, Z., Huang, T., Wang, Y., Wang, C.: Rethinking mobile block for efficient attention-based models. In: *ICCV* (2023) [6](#)
59. Zhang, J., Li, X., Wang, Y., Wang, C., Yang, Y., Liu, Y., Tao, D.: Eatformer: Improving vision transformer inspired by evolutionary algorithm. *IJCV* (2024) [6](#)
60. Zhang, X., Li, S., Li, X., Huang, P., Shan, J., Chen, T.: Destseg: Segmentation guided denoising student-teacher for anomaly detection. In: *CVPR* (2023) [2](#), [3](#), [7](#), [8](#), [9](#), [13](#), [15](#), [16](#), [17](#), [18](#)
61. Zhou, C., Paffenroth, R.C.: Anomaly detection with robust deep autoencoders. In: *ACM SIGKDD* (2017) [2](#), [3](#), [4](#), [5](#), [7](#)
62. Zhou, Q., Li, W., Jiang, L., Wang, G., Zhou, G., Zhang, S., Zhao, H.: Pad: A dataset and benchmark for pose-agnostic anomaly detection. *NeurIPS* (2024) [3](#)
63. Zhu, J., Pang, G.: Toward generalist anomaly detection via in-context residual learning with few-shot sample prompts. *arXiv preprint arXiv:2403.06495* (2024) [3](#)

64. Zhu, J., Shen, Y., Zhao, D., Zhou, B.: In-domain gan inversion for real image editing. In: ECCV (2020) [4](#)
 65. Zou, Y., Jeong, J., Pemula, L., Zhang, D., Dabeer, O.: Spot-the-difference self-supervised pre-training for anomaly detection and segmentation. In: ECCV (2022) [1, 2, 3, 4, 5, 7, 8](#)

Overview

The supplementary material presents the following sections to strengthen the main manuscript:

- Sec. A shows the defect distribution statistics for the proposed general-purpose COCO-AD dataset.
- Sec. B shows extended ablations for hyper-parameters.
- Sec. C shows more qualitative visualization of COCO-AD dataset.
- Sec. D shows more comprehensive results on MVTec 3D AD [6], Uni-Medical [57], and Real-IAD [45] datasets.
- Sec. E shows more quantitative results for each split on COCO-AD dataset.
- Sec. F shows more quantitative results for each category on MVTec AD dataset under the MUAD setting.
- Sec. G shows more quantitative results for each category on VisA dataset under the MUAD setting.
- Sec. H shows more quantitative results for each category on MVTec 3D AD dataset under the MUAD setting.
- Sec. I shows more quantitative results for each category on Uni-Medical dataset under the MUAD setting.
- Sec. J shows more quantitative results for each category on Real-IAD dataset under the MUAD setting. All five view images are used.
- We have attached the full codes and model, including the generation script for the COCO-AD dataset, as well as the InvAD model and log files.

A Statistic Information of COCO-AD

Fig. A1 provides a statistical analysis of the four splits of the COCO-AD dataset across four dimensions to understand its characteristics for the AD task comprehensively. (a) The area proportion of a single object region mainly falls within 2%, with about 90% anomalous areas falling within a 10% proportion. And there are individual data points where the proportion can exceed 50%. (b) A single image may contain multiple defect regions. The distribution trend of each split is similar to (a), but there are slight differences between different splits. (c) The number of objects (defects) in an image is predominantly within two, but a certain proportion can reach more than 20. (d) The ratio of the anomalous region is mostly between 0.5 and 2, but there are certain extreme ratio data, such as those exceeding 10. This illustrates the highly complexity of the COCO-AD dataset in the anomalous regions, which is able to serving as a challenging dataset for the AD field.

Table A1: Ablation for loss function and scheduler.

	Item	mAD _I	mAD _P	mAD _s ²	mAU-PRO	mIoU-max
Loss	Cos _f	98.9	72.0	34.6	94.0	43.8
	Cos _p	98.9	71.6	34.0	94.0	43.0
	L1	98.0	70.5	33.9	93.9	41.9
	MSE	98.9	72.0	34.8	94.1	43.7
Sch.	Cosine	98.9	72.1	34.5	94.2	43.8
	Step	98.9	72.0	34.8	94.1	43.7

B More Ablations for Hyper-parameters

- 1) **Resolution.** The upper part of Fig. A2 shows the result changes of different methods on five comprehensive metrics under resolutions from 64 to 512. Our method significantly improves as the resolution increases, showing a clear advantage over the comparison methods above a resolution of 256×256. Considering the computational load and performance, this paper adopts the default resolution of 256×256 in this field.
- 2) **Training Epoch.** The lower part of Fig. A2 shows the impact of training epochs on the results. Our method converges faster than the comparison methods, achieving nearly stable results with only 100 epochs.

- 3) **Loss Function.** RD [12] and UniAD [52] show significant differences in performance when using different pixel-level constraints. The upper part of Table A1 shows the results of our method under flattened cosine distance, pixel-level cosine distance, L1, and MSE constraints, indicating that our method has strong robustness.

- 4) **Learning Rate Scheduler.** The lower part of Table A1 shows that the cosine scheduler [33], which is effective in other fields, does not significantly differ from the Step strategy in the AD field.

C More Qualitative Visualization of COCO-AD Dataset

Fig. A3 presents more visualization results from the COCO-AD dataset, where general-purpose scenes and complex anomalous attributes demonstrate its highly challenging nature.

D More Quantitative Comprehensive Results on Popular AD Datasets

We further conduct quantitative experiments on MVTec 3D AD, Uni-Medical, and Real-IAD datasets for evaluating different methods comprehensively beyond Table 3 in the main paper. Considering effectiveness and training cost, we only select powerful and representative methods for experiments.

E Quantitative Results for Each Category on COCO-AD

Table A3 shows detailed quantitative single-split results on the COCO-AD dataset.

F Quantitative Results for Each Category on MVTec AD

Table A4 and Table A5 show detailed quantitative single-class results for Textures and Object categories on the MVTec AD dataset.

G Quantitative Results for Each Category on VisA

Table A6, Table A7, and Table A8 show detailed quantitative single-class results for Complex Structure, Multiple Instance Object, and Single Instance categories on VisA dataset.

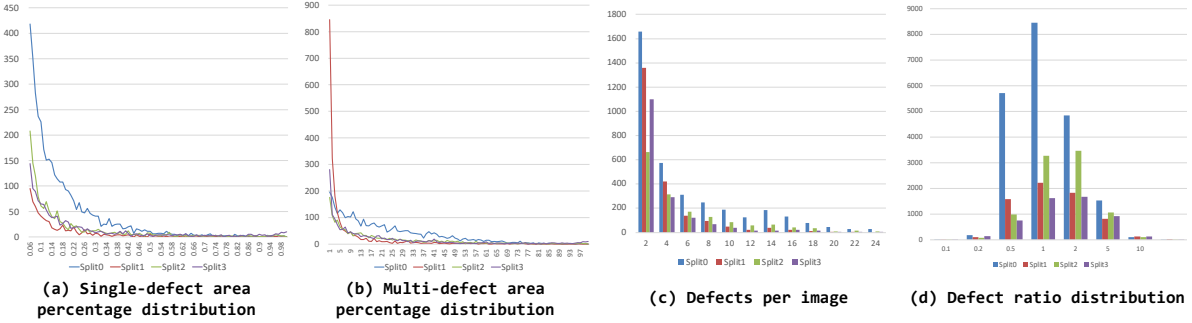


Fig. A1: Statistics of the general-purpose COCO-AD dataset.

Table A2: Different fine-grained multi-class anomaly classification and segmentation results with SoTAs on more AD datasets beyond Table 3. Prefix ‘m’ stands for averaged metric results for all categories. Metrics marked in red are recommended. **Bold** and underline represent optimal and sub-optimal results, respectively.

	Fineness-level	Metric	RD* [12]	UniAD† [52]	SimpleNet* [32]	DiAD [16]	InvAD-lite	InvAD
MVTec 3D AD [6]	Image-level (Classification)	mAU-ROC	77.9	78.9	72.5	84.6	<u>85.3</u>	86.1
		mAP	92.4	93.4	91.0	94.8	<u>95.2</u>	95.8
		mF ₁ -max	91.4	91.4	90.3	95.6	93.0	<u>93.2</u>
	Region-level	mAU-PRO	93.5	88.1	77.6	87.8	<u>94.1</u>	94.7
	Pixel-level (Segmentation)	mAU-ROC	98.4	96.5	93.6	96.4	<u>98.6</u>	98.8
		mAP	29.8	21.2	18.3	25.3	<u>37.2</u>	37.8
		mF ₁ -max	36.4	28.0	25.3	32.3	<u>41.4</u>	42.5
Uni-Medical [57]	Proposed	mF ₁ _{.8} ^{.2}	16.0	12.2	11.0	5.0	<u>21.6</u>	22.0
		mAcc _{.8} ^{.2}	53.1	43.6	<u>52.7</u>	51.4	55.3	50.5
		mIoU _{.8} ^{.2}	9.4	7.0	6.2	2.6	<u>12.9</u>	13.2
		mIoU-max	22.8	16.8	15.0	5.4	<u>26.5</u>	27.5
	Averaged Metrics	mAD_I	87.2	87.9	84.6	91.7	<u>91.2</u>	91.7
		mAD_P	54.9	48.6	45.7	51.3	<u>59.1</u>	59.7
		mAD_S	26.2	20.9	23.3	26.3	29.9	<u>28.6</u>
Real-IAD [45]	Image-level (Classification)	mAU-ROC	75.6	78.5	75.6	85.1	79.5	<u>82.2</u>
		mAP	75.8	75.2	76.9	84.5	78.3	<u>79.6</u>
		mF ₁ -max	78.0	76.6	76.8	81.2	79.1	<u>80.6</u>
	Region-level	mAU-PRO	<u>86.4</u>	85.0	80.5	85.4	85.5	89.6
	Pixel-level (Segmentation)	mAU-ROC	96.5	96.4	95.9	95.9	96.4	97.4
		mAP	38.7	37.6	38.3	38.0	<u>40.1</u>	47.5
		mF ₁ -max	40.1	40.2	39.6	35.6	<u>40.4</u>	47.1
Averaged Metrics	Proposed	mF ₁ _{.8} ^{.2}	16.4	13.3	15.0	18.0	<u>18.3</u>	21.8
		mAcc _{.8} ^{.2}	43.2	37.8	46.5	37.6	40.5	<u>45.2</u>
		mIoU _{.8} ^{.2}	10.0	8.0	9.0	10.4	<u>11.2</u>	13.8
		mIoU-max	27.3	26.8	25.8	25.0	27.6	33.3
	Averaged Metrics	mAD_I	76.5	76.8	76.4	83.6	79.0	80.8
		mAD_P	58.4	58.1	57.9	56.5	<u>59.0</u>	64.0
		mAD_S	23.2	19.7	<u>23.5</u>	22.0	23.3	26.9

H Quantitative Results for Each Category on MVTec 3D AD

Table A9 shows detailed quantitative single-class results on MVTec 3D AD dataset.

I Quantitative Results for Each Category on Uni-Medical

Table A10 shows detailed quantitative single-class results on Uni-Medical dataset.

Table A3: **Quantitative results for each split on COCO-AD dataset.** These are respectively the image-level mAU-ROC/mAP/m F_1 -max, region-level **mAU-PRO**, pixel-level mAU-ROC/mAP/m F_1 -max, the proposed pixel-level m F_1 $_{.8}^2$ /mAcc $_{.8}^2$ /mIoU $_{.8}^2$ /mIoU-max, and averaged **mAD I** /**mAD P** /**mAD $_{.8}^2$** . Subsequent tables will default to this setting.

	Method	mAU-ROC/mAP/m F_1 -max	mAU-PRO	mAU-ROC/mAP/m F_1 -max	m F_1 $_{.8}^2$ /mAcc $_{.8}^2$ /mIoU $_{.8}^2$ /mIoU-max	mAD I / mADP / mAD$_{.8}^2$
Split0	DRÆM* [55]	53.9 / 76.4 / 85.0	12.5	54.0 / 17.7 / 27.7	11.3 / 26.0 / 8.1 / 16.1	71.8 / 33.1 / 15.1
	RD* [12]	65.7 / 81.9 / 85.1	45.9	72.1 / 30.8 / 38.2	17.7 / 34.6 / 10.5 / 23.6	77.6 / 47.0 / 20.9
	UniAD \dagger [52]	66.1 / 84.0 / 85.1	36.5	70.8 / 29.4 / 36.7	11.3 / 22.6 / 6.7 / 22.5	78.4 / 45.6 / 13.5
	DeSTSeg* [60]	59.7 / 79.1 / 85.0	23.5	61.8 / 21.5 / 27.7	1.0 / 0.6 / 0.5 / 16.1	74.6 / 37.0 / 0.7
	SimpleNet* [32]	57.8 / 77.4 / 84.7	26.8	64.0 / 27.4 / 34.4	13.6 / 31.4 / 7.8 / 20.7	73.3 / 41.9 / 17.6
	DiAD [16]	57.5 / 77.5 / 85.3	28.8	67.0 / 33.4 / 26.2	19.7 / 30.6 / 12.4 / 20.1	73.4 / 42.2 / 20.9
	InvAD-lite	77.0 / 90.1 / 85.5	46.8	76.6 / 40.3 / 42.9	21.5 / 38.7 / 13.0 / 27.3	84.2 / 53.3 / 24.4
	InvAD	73.8 / 87.8 / 85.1	51.1	78.9 / 42.6 / 45.6	22.3 / 39.0 / 13.6 / 29.6	82.2 / 55.7 / 25.0
	DRÆM* [55]	51.3 / 43.9 / 60.9	6.8	52.4 / 3.2 / 6.0	3.9 / 18.7 / 3.3 / 3.1	52.0 / 20.5 / 8.6
	RD* [12]	54.9 / 46.8 / 61.1	40.6	70.7 / 6.2 / 11.2	4.4 / 27.6 / 2.3 / 5.9	54.3 / 29.4 / 11.4
Split1	UniAD \dagger [52]	56.1 / 47.8 / 61.1	31.8	70.0 / 6.2 / 11.3	4.0 / 28.9 / 2.1 / 6.0	55.0 / 29.2 / 11.7
	DeSTSeg* [60]	55.6 / 47.9 / 61.2	27.7	69.3 / 6.8 / 11.3	4.0 / 2.5 / 2.0 / 6.0	54.9 / 29.1 / 2.8
	SimpleNet* [32]	51.2 / 42.3 / 59.0	33.0	61.4 / 4.9 / 8.9	5.6 / 34.2 / 2.9 / 4.7	50.8 / 25.1 / 14.2
	DiAD [16]	54.4 / 49.8 / 62.2	28.8	71.3 / 11.8 / 7.8	1.9 / 21.2 / 1.6 / 6.2	55.5 / 30.3 / 8.2
	InvAD-lite	53.7 / 46.8 / 61.0	33.1	72.4 / 7.8 / 12.9	5.6 / 31.7 / 2.9 / 6.9	53.8 / 31.0 / 13.4
	InvAD	55.8 / 48.4 / 60.9	41.7	74.3 / 8.7 / 14.4	7.1 / 38.1 / 3.7 / 7.8	55.0 / 32.5 / 16.3
	DRÆM* [55]	54.5 / 33.4 / 50.4	12.1	50.4 / 6.1 / 11.9	7.5 / 28.3 / 5.8 / 6.3	46.1 / 22.8 / 13.9
	RD* [12]	59.6 / 39.4 / 51.3	42.9	68.4 / 11.6 / 18.9	9.6 / 38.9 / 5.2 / 10.4	50.1 / 33.0 / 17.9
	UniAD \dagger [52]	52.3 / 30.8 / 49.5	27.0	60.9 / 7.7 / 14.7	5.6 / 29.0 / 3.0 / 7.9	44.2 / 27.8 / 12.5
	DeSTSeg* [60]	55.8 / 37.6 / 50.1	26.3	61.1 / 9.8 / 13.9	2.8 / 1.9 / 1.5 / 7.4	47.8 / 28.3 / 2.1
Split2	SimpleNet* [32]	60.1 / 38.5 / 50.7	29.2	57.4 / 8.2 / 14.4	8.5 / 33.9 / 4.5 / 7.8	49.8 / 26.7 / 15.6
	DiAD [16]	63.8 / 43.4 / 52.5	33.2	68.0 / 19.2 / 12.2	8.0 / 29.3 / 5.0 / 10.6	53.2 / 33.1 / 14.1
	InvAD-lite	68.7 / 49.2 / 54.5	41.3	73.2 / 16.4 / 23.1	10.2 / 34.7 / 5.6 / 13.1	57.5 / 37.6 / 16.8
	InvAD	68.2 / 48.0 / 55.0	47.7	75.7 / 16.9 / 24.9	11.3 / 38.2 / 6.2 / 14.2	57.1 / 39.2 / 18.6
	DRÆM* [55]	60.5 / 41.7 / 53.5	15.6	50.4 / 6.5 / 12.4	8.9 / 24.5 / 5.2 / 6.6	51.9 / 23.1 / 12.9
	RD* [12]	53.5 / 36.4 / 51.5	33.4	58.3 / 8.4 / 14.2	7.8 / 34.1 / 4.1 / 7.6	47.1 / 27.0 / 15.3
	UniAD \dagger [52]	50.1 / 33.5 / 51.2	31.4	59.8 / 8.3 / 14.8	5.4 / 24.9 / 2.9 / 8.0	44.9 / 27.6 / 11.1
	DeSTSeg* [60]	53.5 / 36.5 / 51.2	16.8	51.2 / 6.9 / 12.4	1.6 / 0.9 / 0.8 / 6.6	47.1 / 23.5 / 1.1
	SimpleNet* [32]	59.2 / 39.2 / 52.2	21.0	55.3 / 8.2 / 13.9	6.4 / 29.6 / 3.4 / 7.5	50.2 / 25.8 / 13.1
	DiAD [16]	60.1 / 41.4 / 52.9	32.3	65.9 / 17.5 / 10.6	8.6 / 43.4 / 5.3 / 9.6	51.5 / 31.3 / 19.1
Split3	InvAD-lite	59.2 / 40.5 / 52.8	31.6	60.0 / 8.9 / 14.6	7.5 / 31.6 / 4.0 / 7.9	50.8 / 27.8 / 14.4
	InvAD	65.8 / 46.8 / 55.3	39.1	64.1 / 10.5 / 16.8	8.9 / 34.8 / 4.8 / 9.2	56.0 / 30.5 / 16.2

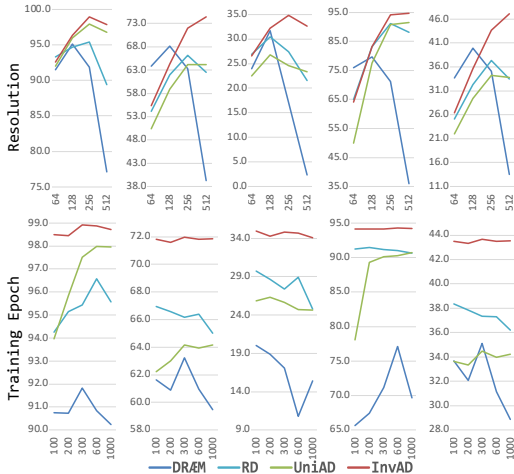
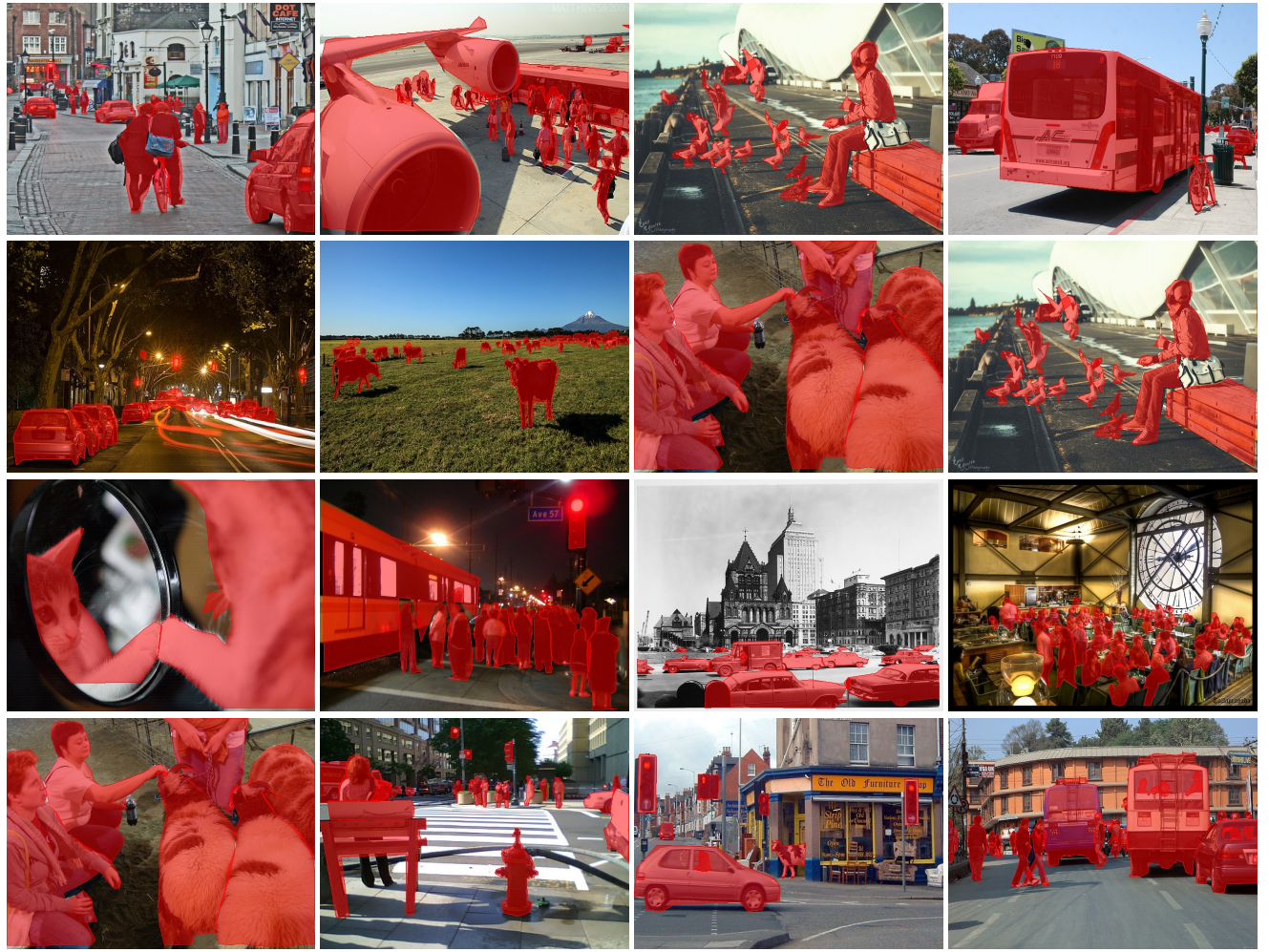


Fig. A2: Ablation of image resolution and training epoch on mAD I , mAD P , mAD $_{.8}^2$, mAU-PRO, and mIoU-max.

J Quantitative Results for Each Category on Real-IAD

Table A11, Table A12, and Table A13 show detailed quantitative single-class results on Real-IAD dataset.



Multiple Object-oriented Defect Per Image General-purpose Scenes
 Pose-/Scale-/Semantic/Appearance-Agnostic Defect for Fair Comparison

Fig. A3: More challenging visualizations of COCO-AD dataset for split0. The red regions represent anomalous objects during testing.

Table A4: **Quantitative results for each class (Textures) on MVTec AD dataset.** These are respectively the image-level mAU-ROC/mAP/m F_1 -max, region-level **mAU-PRO**, pixel-level mAU-ROC/mAP/m F_1 -max, the proposed pixel-level m $F_{1.8}^2$ /mAcc $_{.8}^2$ /mIoU $_{.8}^2$ /**mIoU-max**, and averaged **mAD I** /**mAD P** /**mAD $_{.8}^2$** .

	Method	mAU-ROC/mAP/m F_1 -max	mAU-PRO	mAU-ROC/mAP/m F_1 -max	m $F_{1.8}^2$ /mAcc $_{.8}^2$ /mIoU $_{.8}^2$ / mIoU-max	mADI / mADP / mAD$_{.8}^2$
carpet	DRÆM* [55]	97.2 / 99.1 / 96.7	93.1	98.1 / 78.7 / 73.1	46.5 / 33.7 / 31.9 / 57.6	97.7 / 83.3 / 37.4
	RD* [12]	98.5 / 99.6 / 97.2	95.1	99.0 / 58.5 / 60.5	36.4 / 50.3 / 24.0 / 43.3	98.4 / 72.7 / 36.9
	UniAD \dagger [52]	99.8 / 99.9 / 99.4	94.4	98.4 / 51.4 / 51.5	30.3 / 43.7 / 19.3 / 34.6	99.7 / 67.1 / 31.1
	DeSTSeg* [60]	95.9 / 98.8 / 94.9	89.3	93.6 / 59.9 / 58.9	48.3 / 55.4 / 32.3 / 41.7	96.5 / 70.8 / 45.3
	SimpleNet* [32]	95.7 / 98.7 / 93.2	90.6	97.4 / 38.7 / 43.2	24.5 / 41.1 / 14.6 / 27.5	95.9 / 59.8 / 26.7
	DiAD [16]	99.7 / 96.5 / 91.8	86.6	98.4 / 52.2 / 54.8	12.3 / 34.2 / 6.8 / 15.7	96.0 / 68.5 / 17.8
	InvAD-lite	99.8 / 99.9 / 98.9	95.4	99.1 / 62.2 / 61.3	39.8 / 54.7 / 26.3 / 44.2	99.5 / 74.2 / 40.3
grid	InvAD	98.2 / 99.5 / 96.6	94.9	99.1 / 61.4 / 61.7	40.3 / 54.8 / 26.7 / 44.6	98.1 / 74.1 / 40.6
	DRÆM* [55]	99.2 / 99.7 / 98.2	92.1	99.0 / 44.5 / 46.2	30.7 / 28.2 / 18.8 / 30.0	99.0 / 63.2 / 25.9
	RD* [12]	98.0 / 99.4 / 96.6	97.0	99.2 / 46.0 / 47.4	31.9 / 57.6 / 19.6 / 31.0	98.0 / 64.2 / 36.4
	UniAD \dagger [52]	99.3 / 99.8 / 99.1	92.9	97.7 / 23.7 / 30.4	18.7 / 42.3 / 10.6 / 18.0	99.4 / 50.6 / 23.9
	DeSTSeg* [60]	97.9 / 99.2 / 96.6	86.8	97.0 / 42.1 / 46.9	33.0 / 34.5 / 20.5 / 30.6	97.9 / 62.0 / 29.3
	SimpleNet* [32]	97.6 / 99.2 / 96.4	88.6	96.8 / 20.5 / 27.6	14.8 / 52.2 / 8.3 / 16.0	97.7 / 48.3 / 25.1
	DiAD [16]	94.8 / 98.8 / 95.2	80.5	96.8 / 50.1 / 57.8	5.3 / 23.8 / 2.7 / 5.3	96.3 / 68.2 / 10.6
leather	InvAD-lite	100. / 100. / 100.	96.9	99.3 / 49.7 / 49.8	31.4 / 41.2 / 19.6 / 33.2	100. / 66.3 / 30.7
	InvAD	100. / 100. / 100.	96.3	99.2 / 44.5 / 47.1	28.4 / 35.7 / 17.6 / 30.8	100. / 63.6 / 27.2
	DRÆM* [55]	97.7 / 99.3 / 95.0	88.5	98.9 / 60.3 / 57.4	30.6 / 19.7 / 18.5 / 40.2	97.3 / 72.2 / 22.9
	RD* [12]	100. / 100. / 100.	97.4	99.3 / 38.0 / 45.1	27.6 / 49.9 / 16.8 / 29.1	100. / 60.8 / 31.4
	UniAD \dagger [52]	100. / 100. / 100.	96.8	98.8 / 34.2 / 35.5	20.6 / 40.6 / 11.9 / 21.6	100. / 56.2 / 24.4
	DeSTSeg* [60]	99.2 / 99.8 / 98.9	91.1	99.5 / 71.5 / 66.5	57.6 / 50.1 / 40.9 / 49.8	99.3 / 79.2 / 49.5
	SimpleNet* [32]	100. / 100. / 100.	92.7	98.7 / 28.5 / 32.9	20.3 / 64.5 / 11.6 / 19.7	100. / 53.4 / 32.1
tile	DiAD [16]	89.0 / 97.5 / 95.5	87.2	97.1 / 42.0 / 45.3	5.4 / 38.2 / 2.9 / 7.0	94.0 / 61.5 / 15.5
	InvAD-lite	100. / 100. / 100.	98.5	99.3 / 44.7 / 48.1	32.5 / 70.3 / 19.9 / 31.7	100. / 64.0 / 40.9
	InvAD	100. / 100. / 100.	97.3	99.4 / 47.1 / 49.5	32.6 / 60.6 / 20.1 / 32.9	100. / 65.3 / 37.8
	DRÆM* [55]	100. / 100. / 100.	97.0	99.2 / 93.6 / 86.0	65.4 / 50.8 / 50.0 / 75.4	100. / 92.9 / 55.4
	RD* [12]	98.3 / 99.3 / 96.4	85.8	95.3 / 48.5 / 60.5	26.8 / 33.3 / 17.6 / 43.4	98.0 / 68.1 / 25.9
	UniAD \dagger [52]	99.9 / 99.9 / 99.4	78.4	92.3 / 41.5 / 50.3	20.7 / 25.9 / 13.1 / 33.6	99.7 / 61.4 / 19.9
	DeSTSeg* [60]	97.0 / 98.9 / 95.3	87.1	93.0 / 71.0 / 66.2	41.8 / 28.2 / 27.1 / 49.4	97.1 / 76.7 / 32.4
wood	SimpleNet* [32]	99.3 / 99.8 / 98.8	90.6	95.7 / 60.5 / 59.9	35.8 / 50.3 / 23.6 / 42.7	99.3 / 72.0 / 36.6
	DiAD [16]	99.5 / 99.7 / 97.3	91.5	98.3 / 79.2 / 80.4	22.7 / 33.5 / 13.1 / 19.8	98.8 / 86.0 / 23.1
	InvAD-lite	98.2 / 99.3 / 97.1	80.0	94.4 / 46.5 / 55.5	31.9 / 43.1 / 20.5 / 38.4	98.2 / 65.5 / 31.8
	InvAD	100. / 100. / 100.	86.0	95.7 / 51.0 / 62.2	37.4 / 47.4 / 24.9 / 45.1	100. / 69.6 / 36.6
	DRÆM* [55]	100. / 100. / 100.	94.2	96.9 / 81.4 / 74.6	49.1 / 34.0 / 33.7 / 59.5	100. / 84.3 / 38.9
	RD* [12]	99.2 / 99.8 / 98.3	90.0	95.3 / 47.8 / 51.0	25.9 / 35.0 / 16.2 / 34.3	99.1 / 64.7 / 25.7
	UniAD \dagger [52]	98.9 / 99.7 / 97.5	86.7	93.2 / 37.4 / 42.8	22.2 / 29.4 / 13.4 / 27.2	98.7 / 57.8 / 21.7
SimpleNet* [32]	DeSTSeg* [60]	99.9 / 100. / 99.2	83.4	95.9 / 77.3 / 71.3	36.5 / 24.0 / 23.5 / 55.4	99.7 / 81.5 / 28.0
	DiAD [16]	98.4 / 99.5 / 96.7	76.3	91.4 / 34.8 / 39.7	24.9 / 46.9 / 14.7 / 24.8	98.2 / 55.3 / 28.8
	InvAD-lite	99.1 / 96.0 / 91.6	90.6	97.3 / 30.0 / 38.3	11.2 / 33.1 / 6.0 / 12.4	95.6 / 55.2 / 16.8
	InvAD	97.3 / 99.1 / 96.8	88.3	94.7 / 45.1 / 47.5	29.2 / 51.1 / 18.0 / 31.1	97.7 / 62.4 / 32.8
	InvAD	99.5 / 99.8 / 98.3	90.3	95.5 / 51.2 / 51.8	34.4 / 52.1 / 21.8 / 34.9	99.2 / 66.2 / 36.1

Table A5: Quantitative results for each class (Objects) on MVTec AD dataset. These are respectively the image-level mAU-ROC/mAP/m F_1 -max, region-level mAU-PRO, pixel-level mAU-ROC/mAP/m F_1 -max, the proposed pixel-level m F_1 $_{.8}^2$ /mAcc $_{.8}^2$ /mIoU $_{.8}^2$ /mIoU-max, and averaged mAD I /mAD P /mAD $_{.8}^2$.

	Method	mAU-ROC/mAP/m F_1 -max	mAU-PRO	mAU-ROC/mAP/m F_1 -max	m F_1 $_{.8}^2$ /mAcc $_{.8}^2$ /mIoU $_{.8}^2$ /mIoU-max	mAD I /mAD P /mAD $_{.8}^2$
bottle	DRÆM* [55]	97.3 / 99.2 / 96.1	80.7	91.3 / 62.5 / 56.9	20.6 / 11.9 / 11.7 / 39.8	97.5 / 70.2 / 14.7
	RD* [12]	99.6 / 99.9 / 98.4	94.0	97.8 / 68.2 / 67.6	32.9 / 37.7 / 22.7 / 51.1	99.3 / 77.9 / 31.1
	UniAD \dagger [52]	100. / 100. / 100.	93.1	98.0 / 67.0 / 67.9	22.7 / 26.1 / 15.7 / 51.4	100. / 77.6 / 21.5
	DeSTSeg* [60]	98.7 / 99.6 / 96.8	67.5	93.3 / 61.7 / 56.0	31.8 / 19.8 / 19.3 / 38.9	98.4 / 70.3 / 23.6
	SimpleNet* [32]	100. / 100. / 100.	89.0	97.2 / 53.8 / 62.4	22.8 / 27.8 / 15.1 / 45.4	100. / 71.1 / 21.9
	DiAD [16]	95.7 / 98.5 / 94.5	89.0	95.7 / 46.0 / 51.4	33.6 / 49.4 / 20.7 / 33.0	96.2 / 64.4 / 34.6
	InvAD-lite	100. / 100. / 100.	95.5	98.5 / 75.9 / 73.6	43.9 / 48.5 / 31.7 / 58.3	100. / 82.7 / 41.4
	InvAD	100. / 100. / 100.	95.3	98.6 / 76.6 / 73.2	44.1 / 48.6 / 31.9 / 57.7	100. / 82.8 / 41.5
cable	DRÆM* [55]	61.1 / 74.0 / 76.3	40.1	75.9 / 14.7 / 17.8	2.0 / 1.1 / 1.0 / 9.8	70.5 / 36.1 / 1.4
	RD* [12]	84.1 / 89.5 / 82.5	75.1	85.1 / 26.3 / 33.6	18.0 / 27.6 / 10.3 / 20.2	85.4 / 48.3 / 18.6
	UniAD \dagger [52]	94.8 / 97.0 / 90.7	86.1	96.9 / 45.4 / 50.4	21.5 / 37.5 / 13.1 / 33.7	94.2 / 64.2 / 24.0
	DeSTSeg* [60]	89.5 / 94.6 / 85.9	49.4	89.3 / 37.5 / 40.5	19.9 / 12.5 / 11.4 / 25.4	90.0 / 55.8 / 14.6
	SimpleNet* [32]	97.5 / 98.5 / 94.7	85.4	96.7 / 42.4 / 51.2	20.6 / 36.9 / 12.6 / 34.4	96.9 / 63.4 / 23.4
	DiAD [16]	90.7 / 99.7 / 97.9	95.0	97.9 / 60.6 / 59.6	20.2 / 45.3 / 11.6 / 20.1	96.1 / 72.7 / 25.7
	InvAD-lite	97.8 / 98.6 / 95.3	86.5	90.8 / 38.5 / 47.0	21.9 / 29.3 / 13.3 / 30.7	97.2 / 58.8 / 21.5
	InvAD	98.8 / 99.3 / 95.7	92.3	97.5 / 48.8 / 53.3	27.7 / 39.3 / 17.2 / 36.4	97.9 / 66.5 / 28.1
capsule	DRÆM* [55]	70.9 / 92.5 / 90.5	27.3	50.5 / 6.0 / 10.0	0.6 / 0.3 / 0.3 / 5.3	84.6 / 22.2 / 0.4
	RD* [12]	94.1 / 96.9 / 96.9	94.8	98.8 / 43.4 / 50.1	23.7 / 32.0 / 14.6 / 33.4	96.0 / 64.1 / 23.4
	UniAD \dagger [52]	93.7 / 98.4 / 96.3	92.1	98.8 / 45.6 / 47.7	28.4 / 44.9 / 17.4 / 31.3	96.1 / 64.0 / 30.2
	DeSTSeg* [60]	82.8 / 95.9 / 92.6	62.1	95.8 / 47.9 / 48.9	27.9 / 18.1 / 16.7 / 32.4	90.4 / 64.2 / 20.9
	SimpleNet* [32]	90.7 / 97.9 / 93.5	84.5	98.5 / 35.4 / 44.3	21.6 / 51.9 / 12.9 / 28.4	94.0 / 59.4 / 28.8
	DiAD [16]	99.7 / 99.9 / 99.2	95.0	99.0 / 78.7 / 72.8	13.1 / 29.2 / 7.2 / 13.7	99.6 / 83.5 / 16.5
	InvAD-lite	96.1 / 99.2 / 95.3	92.9	98.6 / 43.3 / 47.5	25.7 / 29.2 / 15.7 / 31.2	96.9 / 63.1 / 23.5
	InvAD	97.8 / 99.5 / 96.3	95.3	98.9 / 46.5 / 50.8	24.8 / 26.2 / 15.4 / 34.0	97.9 / 65.4 / 22.1
hazelnut	DRÆM* [55]	94.7 / 97.5 / 92.3	78.7	96.5 / 70.0 / 60.5	11.7 / 6.4 / 6.4 / 43.4	94.8 / 75.7 / 8.2
	RD* [12]	60.8 / 69.8 / 86.4	92.7	97.9 / 36.2 / 51.6	5.5 / 4.8 / 3.3 / 34.8	72.3 / 61.9 / 4.5
	UniAD \dagger [52]	100. / 100. / 100.	94.1	98.0 / 53.8 / 56.3	25.9 / 50.8 / 16.2 / 39.2	100. / 69.4 / 31.0
	DeSTSeg* [60]	98.8 / 99.2 / 98.6	84.5	98.2 / 65.8 / 61.6	39.2 / 27.3 / 25.3 / 44.5	98.9 / 75.2 / 30.6
	SimpleNet* [32]	99.9 / 100. / 99.3	87.4	98.4 / 44.6 / 51.4	21.9 / 37.8 / 13.5 / 34.6	99.7 / 64.8 / 24.4
	DiAD [16]	99.8 / 99.6 / 97.4	90.0	95.1 / 15.6 / 31.7	21.3 / 51.4 / 12.3 / 23.4	98.9 / 47.5 / 28.3
	InvAD-lite	100. / 100. / 100.	95.4	98.8 / 56.5 / 61.8	35.1 / 63.2 / 22.9 / 44.7	100. / 72.4 / 40.4
	InvAD	100. / 100. / 100.	96.5	98.9 / 59.8 / 62.3	38.9 / 64.9 / 25.7 / 45.2	100. / 73.7 / 43.2
metal_nut	DRÆM* [55]	81.8 / 95.0 / 92.0	66.4	74.4 / 31.1 / 21.0	4.1 / 2.1 / 2.1 / 11.7	89.6 / 42.2 / 2.8
	RD* [12]	100. / 100. / 99.5	91.9	93.8 / 62.3 / 65.4	28.5 / 39.5 / 18.8 / 48.6	99.8 / 73.8 / 28.9
	UniAD \dagger [52]	98.3 / 99.5 / 98.4	81.8	93.3 / 50.9 / 63.6	24.5 / 33.0 / 15.9 / 46.7	98.7 / 69.3 / 24.5
	DeSTSeg* [60]	92.9 / 98.4 / 92.2	53.0	84.2 / 42.0 / 22.8	8.8 / 4.7 / 4.6 / 12.9	94.5 / 49.7 / 6.0
	SimpleNet* [32]	96.9 / 99.3 / 96.1	85.2	98.0 / 83.1 / 79.4	40.4 / 54.4 / 29.4 / 65.9	97.4 / 86.8 / 41.4
	DiAD [16]	95.1 / 99.1 / 94.4	91.6	96.2 / 60.7 / 60.0	53.7 / 50.6 / 38.3 / 57.1	96.2 / 72.3 / 47.5
	InvAD-lite	99.7 / 99.9 / 99.5	93.4	97.3 / 78.6 / 80.4	43.9 / 53.2 / 32.0 / 67.2	99.7 / 85.4 / 43.0
	InvAD	100. / 100. / 100.	93.4	97.8 / 81.5 / 82.0	44.5 / 50.8 / 33.6 / 69.4	100. / 87.1 / 43.0
pill	DRÆM* [55]	76.2 / 94.9 / 92.5	53.9	93.9 / 59.2 / 44.1	0.5 / 0.3 / 0.3 / 28.3	87.9 / 65.7 / 0.4
	RD* [12]	97.5 / 99.6 / 96.8	95.8	97.5 / 63.4 / 65.2	25.9 / 37.8 / 17.1 / 48.4	98.0 / 75.4 / 26.9
	UniAD \dagger [52]	94.4 / 99.0 / 95.4	95.3	96.1 / 44.5 / 52.4	18.1 / 39.4 / 11.0 / 35.5	96.3 / 64.3 / 22.8
	DeSTSeg* [60]	77.1 / 94.4 / 91.7	27.9	96.2 / 61.7 / 41.8	10.6 / 5.8 / 5.7 / 26.4	87.7 / 66.6 / 7.4
	SimpleNet* [32]	88.2 / 97.7 / 92.5	81.9	96.5 / 72.4 / 67.7	33.5 / 32.4 / 22.2 / 51.2	92.8 / 78.9 / 29.4
	DiAD [16]	99.4 / 99.9 / 98.3	90.6	98.6 / 42.2 / 46.4	24.8 / 53.4 / 14.9 / 33.0	99.2 / 62.4 / 31.0
	InvAD-lite	97.0 / 99.5 / 96.8	95.9	97.9 / 69.5 / 69.3	29.1 / 35.6 / 19.9 / 53.1	97.8 / 78.9 / 28.2
	InvAD	98.5 / 99.7 / 97.8	96.2	98.1 / 69.9 / 69.8	34.9 / 43.2 / 24.0 / 53.6	98.7 / 79.3 / 34.0
screw	DRÆM* [55]	87.7 / 95.7 / 89.9	55.2	90.0 / 33.8 / 40.7	13.8 / 8.3 / 7.8 / 25.5	91.1 / 54.8 / 10.0
	RD* [12]	97.7 / 99.3 / 95.8	96.8	99.4 / 40.2 / 44.7	22.7 / 63.9 / 13.7 / 28.7	97.6 / 61.4 / 33.4
	UniAD \dagger [52]	95.3 / 98.5 / 92.9	95.2	99.2 / 37.4 / 42.3	16.5 / 54.1 / 9.7 / 26.8	95.6 / 59.6 / 26.8
	DeSTSeg* [60]	69.9 / 88.4 / 85.4	47.3	93.8 / 19.9 / 25.3	14.6 / 9.4 / 8.1 / 14.5	81.2 / 46.3 / 10.7
	SimpleNet* [32]	76.7 / 90.5 / 87.7	84.0	96.5 / 15.9 / 23.2	8.8 / 65.2 / 4.8 / 13.1	85.0 / 45.2 / 26.3
	DiAD [16]	98.5 / 99.8 / 97.7	94.0	96.6 / 66.0 / 64.1	3.3 / 43.1 / 1.7 / 4.3	98.7 / 75.6 / 16.0
	InvAD-lite	92.4 / 96.6 / 93.8	97.6	99.5 / 49.3 / 51.5	27.2 / 58.8 / 16.9 / 34.6	94.3 / 66.8 / 34.3
	InvAD	97.2 / 99.0 / 95.5	97.5	99.6 / 48.6 / 50.6	28.1 / 50.7 / 17.4 / 33.9	97.2 / 66.3 / 32.1
toothbrush	DRÆM* [55]	90.8 / 96.8 / 90.0	68.9	97.3 / 55.2 / 55.8	21.3 / 13.3 / 12.5 / 38.7	92.5 / 69.4 / 15.7
	RD* [12]	97.2 / 99.0 / 94.7	92.0	99.0 / 53.6 / 58.8	32.5 / 65.9 / 20.8 / 41.6	97.0 / 70.5 / 39.7
	UniAD \dagger [52]	89.7 / 95.3 / 95.2	87.9	98.4 / 37.8 / 49.1	25.0 / 43.9 / 15.2 / 32.6	93.4 / 61.8 / 28.0
	DeSTSeg* [60]	71.7 / 89.3 / 84.5	30.9	96.2 / 52.9 / 58.8	39.7 / 29.9 / 25.6 / 41.6	81.8 / 69.3 / 31.7
	SimpleNet* [32]	89.7 / 95.7 / 92.3	87.4	98.4 / 46.9 / 52.5	31.5 / 64.0 / 19.7 / 35.6	92.6 / 65.9 / 38.4
	DiAD [16]	99.8 / 99.7 / 97.6	91.3	98.8 / 56.1 / 62.3	11.2 / 46.8 / 6.0 / 9.7	99.0 / 72.4 / 21.3
	InvAD-lite	96.9 / 98.8 / 95.2	91.5	98.9 / 46.1 / 58.4	34.7 / 58.2 / 22.5 / 41.2	97.0 / 67.8 / 38.5
	InvAD	94.7 / 97.8 / 95.2	91.2	99.1 / 55.4 / 60.8	42.8 / 70.3 / 28.4 / 43.7	95.9 / 71.8 / 47.2
transistor	DRÆM* [55]	77.2 / 77.4 / 71.1	39.0	68.0 / 23.6 / 15.1	2.4 / 1.2 / 1.2 / 8.2	75.2 / 35.6 / 1.6
	RD* [12]	94.2 / 95.2 / 90.0	74.7	85.9 / 42.3 / 45.2	23.5 / 29.1 / 14.2 / 29.2	93.1 / 57.8 / 22.3
	UniAD \dagger [52]	99.8 / 99.8 / 97.5	93.5	97.4 / 61.2 / 63.0	23.0 / 28.0 / 15.2 / 46.0	99.0 / 73.9 / 22.1
	DeSTSeg* [60]	78.2 / 79.5 / 68.8	43.9	73.6 / 38.4 / 39.2	19.2 / 10.9 / 10.7 / 24.4	75.5 / 50.4 / 13.6
	SimpleNet* [32]	99.2 / 98.7 / 97.6	83.2	95.8 / 58.2 / 56.0	29.8 / 39.5 / 18.8 / 38.9	98.5 / 70.0 / 29.4
	DiAD [16]	96.8 / 99.9 / 98.4	90.7	92.4 / 65.7 / 64.1	44.7 / 47.9 / 30.4 / 51.9	98.4 / 74.1 / 41.0
	InvAD-lite	98.3 / 97.9 / 92.3	86.8	94.6 / 60.0 / 57.3	30.1 / 29.1 / 19.5 / 40.2	96.2 / 70.6 / 26.2
	InvAD	99.8 / 99.8 / 97.6	94.3	97.3 / 70.7 / 68.5	36.5 / 34.7 / 24.9 / 52.1	99.1 / 78.8 / 32.0
zipper	DRÆM* [55]	99.9 / 100. / 99.2	91.9	98.6 / 74.3 / 69.3	27.5 / 18.1 / 17.2 / 53.0	99.7 / 80.7 / 20.9
	RD* [12]	99.5 / 99.9 / 99.2	94.1	98.5 / 53.9 / 60.3	25.8 / 32.6 / 16.7 / 43.1	99.5 / 70.9 / 25.0
	UniAD \dagger [52]	98.6 / 99.6 / 97.1	92.6	98.0 / 45.0 / 51.9	17.9 / 23.3 / 11.1 / 35.0	98.4 / 65.0 / 17.4
	DeSTSeg* [60]	88.4 / 96.3 / 93.1	66.9	97.3 / 64.7 / 59.2	17.4 / 10.1 / 10.0 / 42.1	92.6 / 73.7 / 12.5
	SimpleNet* [32]	99.0 / 99.7 / 98.3	90.7	97.9 / 53.4 / 54.6	28.4 / 50.0 / 17.9 / 37.5	99.0 / 68.6 / 32.1
	DiAD [16]	99.7 / 100. / 100.	97.5	93.3 / 43.3 / 43.5	10.1 / 31.1 / 5.5 / 13.8	99.9 / 60.0 / 15.6
	InvAD-lite	98.9 / 99.7 / 97.5	95.3	98.6 / 59.7 / 62.7	32.5 / 41.5 / 21.3 / 45.6	98.7 / 73.7 / 31.8
	InvAD	99.7 / 99.9 / 99.2	94.6	98.4 / 51.2 / 58.0	23.3 / 24.4 / 14.9 / 40.9	99.6 / 69.2 / 20.9

Table A6: Quantitative results for each class (Complex Structure) on VisA dataset. These are respectively the image-level mAU-ROC/mAP/m F_1 -max, region-level mAU-PRO, pixel-level mAU-ROC/mAP/m F_1 -max, the proposed pixel-level m F_1 $_{.8}^2$ /mAcc $_{.8}^2$ /mIoU $_{.8}^2$ /mIoU-max, and averaged mAD I /mAD P /mAD $_{.8}^2$.

	Method	mAU-ROC/mAP/m F_1 -max	mAU-PRO	mAU-ROC/mAP/m F_1 -max	m F_1 $_{.8}^2$ /mAcc $_{.8}^2$ /mIoU $_{.8}^2$ /mIoU-max	mAD I /mAD P /mAD $_{.8}^2$
pcb1	DRÆM* [55]	71.9 / 72.3 / 70.0	52.9	94.7 / 31.9 / 37.3	15.3 / 9.6 / 8.7 / 22.9	71.4 / 54.6 / 11.2
	RD* [12]	96.2 / 95.5 / 91.9	95.8	99.4 / 66.2 / 62.4	35.6 / 61.2 / 23.4 / 45.3	94.5 / 76.0 / 40.1
	UniAD \dagger [52]	94.2 / 92.9 / 90.8	88.8	99.2 / 59.6 / 59.6	29.5 / 51.3 / 19.1 / 42.5	92.6 / 72.8 / 33.3
	DeSTSeg* [60]	87.6 / 83.1 / 83.7	83.2	95.8 / 46.4 / 49.0	32.4 / 52.1 / 17.0 / 32.4	84.8 / 63.7 / 33.8
	SimpleNet* [32]	91.6 / 91.9 / 86.0	83.6	99.2 / 86.1 / 78.8	38.8 / 51.4 / 27.5 / 65.1	89.8 / 88.0 / 39.2
	DiAD [16]	88.1 / 88.7 / 80.7	80.2	98.7 / 49.6 / 52.8	1.4 / 39.1 / 0.7 / 1.3	85.8 / 67.0 / 13.7
	InvAD-lite	95.7 / 93.4 / 92.3	96.4	99.8 / 78.9 / 72.7	47.3 / 57.6 / 32.9 / 57.1	93.8 / 83.8 / 45.9
	InvAD	96.4 / 96.1 / 93.1	95.6	99.8 / 80.7 / 76.2	47.6 / 57.2 / 33.6 / 61.6	95.2 / 85.6 / 46.1
pcb2	DRÆM* [55]	78.5 / 78.3 / 76.3	66.2	92.3 / 10.0 / 18.6	7.1 / 5.1 / 3.8 / 10.3	77.7 / 40.3 / 5.3
	RD* [12]	97.8 / 97.8 / 94.2	90.8	98.0 / 22.3 / 30.0	16.5 / 51.8 / 9.3 / 17.7	96.6 / 50.1 / 25.9
	UniAD \dagger [52]	91.1 / 91.6 / 85.1	82.2	98.0 / 9.2 / 16.9	9.9 / 45.8 / 5.3 / 9.2	89.3 / 41.4 / 20.3
	DeSTSeg* [60]	86.5 / 85.8 / 82.6	79.9	97.3 / 14.6 / 28.2	25.0 / 55.4 / 11.3 / 16.4	85.0 / 46.7 / 30.6
	SimpleNet* [32]	92.4 / 93.3 / 84.5	85.7	96.6 / 8.9 / 18.6	8.4 / 58.4 / 4.5 / 10.3	90.1 / 41.4 / 23.8
	DiAD [16]	91.4 / 91.4 / 84.7	67.0	95.2 / 7.5 / 16.7	7.3 / 59.1 / 3.9 / 8.9	89.2 / 39.8 / 23.4
	InvAD-lite	94.5 / 94.6 / 88.8	90.9	98.9 / 11.7 / 22.8	15.1 / 43.5 / 8.3 / 12.9	92.6 / 44.5 / 22.3
	InvAD	97.1 / 97.1 / 92.9	91.6	99.0 / 15.2 / 24.0	16.1 / 37.7 / 8.9 / 13.6	95.7 / 46.1 / 20.9
pcb3	DRÆM* [55]	76.6 / 77.5 / 74.8	43.0	90.8 / 14.1 / 24.4	12.1 / 9.5 / 6.5 / 13.9	76.3 / 43.1 / 9.4
	RD* [12]	96.4 / 96.2 / 91.0	93.9	97.9 / 26.2 / 35.2	21.2 / 56.6 / 12.3 / 21.4	94.5 / 53.1 / 30.0
	UniAD \dagger [52]	82.2 / 83.2 / 77.5	79.3	98.2 / 13.3 / 24.0	13.8 / 50.4 / 7.6 / 13.6	81.0 / 45.2 / 23.9
	DeSTSeg* [60]	93.7 / 95.1 / 87.0	62.4	97.7 / 28.1 / 33.4	31.9 / 57.5 / 15.3 / 20.0	91.9 / 53.1 / 34.9
	SimpleNet* [32]	89.1 / 91.1 / 82.6	85.1	97.2 / 31.0 / 36.1	17.7 / 57.1 / 10.2 / 22.0	87.6 / 54.8 / 28.3
	DiAD [16]	86.2 / 87.6 / 77.6	68.9	96.7 / 8.0 / 18.8	17.9 / 56.1 / 10.7 / 33.4	83.8 / 41.2 / 28.2
	InvAD-lite	94.7 / 95.0 / 87.2	92.2	99.2 / 17.0 / 29.0	20.3 / 48.0 / 11.5 / 17.0	92.3 / 48.4 / 26.6
	InvAD	97.0 / 97.4 / 92.4	92.0	99.2 / 16.0 / 28.4	20.6 / 49.6 / 11.6 / 16.6	95.6 / 47.9 / 27.3
pcb4	DRÆM* [55]	97.4 / 97.6 / 93.5	75.7	94.4 / 31.0 / 37.6	9.0 / 5.5 / 5.0 / 23.2	96.2 / 54.3 / 6.5
	RD* [12]	99.9 / 99.9 / 99.0	88.7	97.8 / 31.4 / 37.0	17.9 / 39.9 / 10.4 / 22.7	99.6 / 55.4 / 22.7
	UniAD \dagger [52]	99.0 / 99.1 / 95.5	82.9	97.2 / 29.4 / 33.5	17.2 / 41.5 / 9.9 / 20.1	97.9 / 53.4 / 22.9
	DeSTSeg* [60]	97.8 / 97.8 / 92.7	76.9	95.8 / 53.0 / 53.2	25.8 / 54.1 / 17.4 / 36.2	96.1 / 67.3 / 32.4
	SimpleNet* [32]	97.0 / 97.0 / 93.5	61.1	93.9 / 23.9 / 32.9	10.1 / 30.5 / 5.7 / 19.7	95.8 / 50.2 / 15.4
	DiAD [16]	99.6 / 99.5 / 97.0	85.0	97.0 / 17.6 / 27.2	12.2 / 52.3 / 7.0 / 18.0	98.7 / 47.3 / 23.8
	InvAD-lite	99.8 / 99.8 / 98.0	89.6	98.8 / 51.1 / 49.8	27.5 / 33.3 / 17.2 / 33.2	99.2 / 66.6 / 26.0
	InvAD	99.8 / 99.8 / 98.0	89.9	98.6 / 46.6 / 45.2	29.8 / 37.6 / 18.3 / 29.2	99.2 / 63.5 / 28.6

Table A7: Quantitative results for each class (Multiple Instances) on VisA dataset. These are respectively the image-level mAU-ROC/mAP/m F_1 -max, region-level mAU-PRO, pixel-level mAU-ROC/mAP/m F_1 -max, the proposed pixel-level m F_1 $_{.8}^2$ /mAcc $_{.8}^2$ /mIoU $_{.8}^2$ /mIoU-max, and averaged mAD I /mAD P /mAD $_{.8}^2$.

	Method	mAU-ROC/mAP/m F_1 -max	mAU-PRO	mAU-ROC/mAP/m F_1 -max	m F_1 $_{.8}^2$ /mAcc $_{.8}^2$ /mIoU $_{.8}^2$ /mIoU-max	mAD I /mAD P /mAD $_{.8}^2$
macaroni1	DRÆM* [55]	69.8 / 68.6 / 70.9	67.0	95.0 / 19.1 / 24.1	15.9 / 9.9 / 8.7 / 13.7	69.8 / 46.1 / 11.5
	RD* [12]	75.9 / 61.5 / 76.8	95.3	99.4 / 2.9 / 6.9	2.3 / 7.7 / 1.1 / 3.6	71.4 / 36.4 / 3.7
	UniAD \dagger [52]	82.8 / 79.3 / 75.7	92.6	99.0 / 7.6 / 16.1	7.1 / 37.0 / 3.8 / 8.7	79.3 / 40.9 / 16.0
	DeSTSeg* [60]	76.6 / 69.0 / 71.0	62.4	99.1 / 5.8 / 13.4	11.0 / 18.8 / 5.8 / 7.2	72.2 / 39.4 / 11.9
	SimpleNet* [32]	85.9 / 82.5 / 73.1	92.0	98.9 / 3.5 / 8.4	4.1 / 52.3 / 2.1 / 4.4	80.5 / 36.9 / 19.5
	DiAD [16]	85.7 / 85.2 / 78.8	68.5	94.1 / 10.2 / 16.7	41.9 / 59.6 / 27.8 / 44.7	83.2 / 40.3 / 43.1
	InvAD-lite	93.8 / 91.4 / 87.8	96.9	99.7 / 19.8 / 27.3	17.5 / 42.5 / 9.8 / 15.8	91.0 / 48.9 / 23.3
	InvAD	94.1 / 92.5 / 88.0	96.6	99.7 / 20.8 / 29.4	16.9 / 42.4 / 9.5 / 17.2	91.5 / 50.0 / 22.9
macaroni2	DRÆM* [55]	59.4 / 60.7 / 68.1	65.3	94.6 / 3.9 / 12.5	2.1 / 1.2 / 1.1 / 6.6	62.7 / 37.0 / 1.5
	RD* [12]	88.3 / 84.5 / 83.8	97.4	99.7 / 13.2 / 21.8	9.8 / 61.9 / 5.3 / 12.3	85.5 / 44.9 / 25.7
	UniAD \dagger [52]	76.0 / 75.8 / 70.2	87.0	97.3 / 5.1 / 12.2	4.7 / 46.1 / 2.5 / 6.5	74.0 / 38.2 / 17.8
	DeSTSeg* [60]	68.9 / 62.1 / 67.7	70.0	98.5 / 6.3 / 14.4	10.8 / 13.4 / 5.7 / 7.7	66.2 / 39.7 / 10.0
	SimpleNet* [32]	68.3 / 54.3 / 59.7	77.8	93.2 / 0.6 / 3.9	1.0 / 59.6 / 0.5 / 2.0	60.8 / 32.6 / 20.4
	DiAD [16]	62.5 / 57.4 / 69.6	73.1	93.6 / 0.9 / 2.8	0.0 / 8.4 / 0.0 / 0.0	63.2 / 32.4 / 2.8
	InvAD-lite	88.0 / 85.1 / 81.9	97.8	99.7 / 12.2 / 18.8	11.8 / 46.0 / 6.4 / 10.4	85.0 / 43.6 / 21.4
	InvAD	85.8 / 83.2 / 80.6	97.2	99.6 / 11.4 / 18.6	10.8 / 45.0 / 5.8 / 10.2	83.2 / 43.2 / 20.5
capsules	DRÆM* [55]	83.4 / 91.1 / 82.1	62.9	97.1 / 27.8 / 33.8	22.5 / 17.9 / 12.9 / 20.3	85.5 / 52.9 / 17.8
	RD* [12]	82.2 / 90.4 / 81.3	93.1	99.4 / 60.4 / 60.8	27.6 / 66.5 / 18.0 / 43.7	84.6 / 73.5 / 37.4
	UniAD \dagger [52]	70.3 / 83.2 / 77.8	72.2	97.4 / 40.4 / 44.7	13.8 / 62.4 / 8.2 / 28.8	77.1 / 60.8 / 28.1
	DeSTSeg* [60]	87.1 / 93.0 / 84.2	76.7	96.9 / 33.2 / 39.1	24.4 / 37.9 / 15.9 / 18.3	88.1 / 56.4 / 26.1
	SimpleNet* [32]	74.1 / 82.8 / 74.6	73.7	97.1 / 52.9 / 53.3	19.6 / 55.4 / 12.3 / 36.3	77.2 / 67.8 / 29.1
	DiAD [16]	58.2 / 69.0 / 78.5	77.9	97.3 / 10.0 / 21.0	0.0 / 27.1 / 0.0 / 0.0	68.6 / 42.8 / 9.0
	InvAD-lite	90.7 / 94.0 / 88.8	94.7	99.3 / 59.7 / 58.1	33.8 / 61.9 / 21.9 / 40.9	91.2 / 72.4 / 39.2
	InvAD	90.5 / 94.3 / 88.3	94.7	99.7 / 68.1 / 64.7	39.2 / 63.0 / 26.5 / 47.8	91.0 / 77.5 / 42.9
candle	DRÆM* [55]	69.3 / 73.9 / 68.1	65.6	82.2 / 10.1 / 19.0	4.1 / 2.2 / 2.1 / 10.5	70.4 / 37.1 / 2.8
	RD* [12]	92.3 / 92.9 / 86.0	94.9	99.1 / 25.3 / 35.8	16.9 / 38.4 / 9.8 / 21.8	90.4 / 53.4 / 21.7
	UniAD \dagger [52]	95.8 / 96.2 / 90.0	93.0	99.0 / 23.6 / 32.6	16.0 / 46.7 / 9.1 / 19.5	94.0 / 51.7 / 23.9
	DeSTSeg* [60]	94.9 / 94.8 / 89.2	69.0	98.7 / 39.9 / 45.8	30.9 / 37.4 / 21.9 / 29.7	93.0 / 61.5 / 30.1
	SimpleNet* [32]	84.1 / 73.3 / 76.6	87.6	97.6 / 8.4 / 16.5	7.6 / 46.5 / 4.1 / 9.0	78.0 / 40.8 / 19.4
	DiAD [16]	92.8 / 92.0 / 87.6	89.4	97.3 / 12.8 / 22.8	20.3 / 54.0 / 12.0 / 24.6	90.8 / 44.3 / 28.8
	InvAD-lite	96.6 / 96.8 / 91.3	95.9	99.1 / 21.4 / 30.8	18.5 / 34.0 / 10.5 / 18.2	94.9 / 50.4 / 21.0
	InvAD	94.8 / 94.1 / 90.6	95.4	99.3 / 23.6 / 34.5	17.8 / 33.7 / 10.2 / 20.9	93.2 / 52.5 / 20.6

Table A8: **Quantitative results for each class (Single Instance) on VisA dataset.** These are respectively the image-level mAU-ROC/mAP/m F_1 -max, region-level **mAU-PRO**, pixel-level mAU-ROC/mAP/m F_1 -max, the proposed pixel-level m F_1 $_{.8}^2$ /mAcc $_{.8}^2$ /mIoU $_{.8}^2$ /**mIoU-max**, and averaged **mAD I** /**mAD P** /**mAD $_{.8}^2$** .

	Method	mAU-ROC/mAP/m F_1 -max	mAU-PRO	mAU-ROC/mAP/m F_1 -max	m F_1 $_{.8}^2$ /mAcc $_{.8}^2$ /mIoU $_{.8}^2$ / mIoU-max	mADI / mADP / mAD$_{.8}^2$
cashew	DRÆM* [55]	81.7 / 89.7 / 87.3	38.5	80.7 / 9.9 / 15.8	1.6 / 0.8 / 0.8 / 8.6	86.2 / 35.5 / 1.1
	RD* [12]	92.0 / 95.8 / 90.7	86.2	91.7 / 44.2 / 49.7	20.2 / 29.4 / 12.5 / 33.0	92.8 / 61.9 / 20.7
	UniAD \dagger [52]	94.3 / 97.2 / 91.1	88.5	99.0 / 56.2 / 58.9	25.2 / 33.1 / 16.4 / 41.8	94.2 / 71.4 / 24.9
	DeSTSeg* [60]	92.0 / 96.1 / 88.1	66.3	87.9 / 47.6 / 52.1	32.4 / 30.5 / 25.1 / 35.2	92.1 / 62.5 / 29.3
	SimpleNet* [32]	88.0 / 91.3 / 84.7	84.1	98.9 / 68.9 / 66.0	31.3 / 52.5 / 20.9 / 49.2	88.0 / 77.9 / 34.9
	DiAD [16]	91.5 / 95.7 / 89.7	61.8	90.9 / 53.1 / 60.9	6.3 / 52.7 / 3.3 / 6.5	92.3 / 68.3 / 20.8
	InvAD-lite	92.3 / 96.2 / 89.3	89.7	94.7 / 52.9 / 56.0	30.2 / 37.9 / 19.3 / 38.9	92.6 / 67.9 / 29.1
chewinggum	InvAD	96.6 / 98.5 / 94.9	90.3	96.4 / 59.1 / 61.5	36.8 / 44.8 / 24.3 / 44.4	96.7 / 72.3 / 35.3
	DRÆM* [55]	93.7 / 97.2 / 91.0	41.0	91.1 / 62.4 / 63.3	44.5 / 33.8 / 30.0 / 46.4	94.0 / 72.3 / 36.1
	RD* [12]	94.9 / 97.5 / 92.1	76.9	98.7 / 59.9 / 61.7	29.5 / 63.9 / 19.4 / 44.6	94.8 / 73.4 / 37.6
	UniAD \dagger [52]	97.5 / 98.9 / 96.4	85.0	99.1 / 59.5 / 58.0	27.3 / 58.8 / 17.6 / 40.8	97.6 / 72.2 / 34.6
	DeSTSeg* [60]	95.8 / 98.3 / 94.7	68.3	98.8 / 86.9 / 81.0	38.7 / 68.8 / 31.5 / 48.0	96.3 / 88.9 / 46.3
	SimpleNet* [32]	96.4 / 98.2 / 93.8	78.3	97.9 / 26.8 / 29.8	17.8 / 59.7 / 10.1 / 17.5	96.1 / 51.5 / 29.2
	DiAD [16]	99.1 / 99.5 / 95.9	59.5	94.7 / 11.9 / 25.8	5.7 / 40.3 / 2.9 / 5.7	98.2 / 44.1 / 16.3
fryum	InvAD-lite	97.9 / 99.0 / 95.3	79.6	98.3 / 55.2 / 57.2	28.9 / 61.1 / 18.6 / 40.1	97.4 / 70.2 / 36.2
	InvAD	98.3 / 99.1 / 95.9	80.7	98.7 / 60.0 / 62.5	33.6 / 64.6 / 22.1 / 45.5	97.8 / 73.7 / 40.1
	DRÆM* [55]	89.2 / 95.0 / 86.6	69.5	92.4 / 38.8 / 38.6	3.5 / 1.8 / 1.8 / 23.9	90.3 / 56.6 / 2.4
	RD* [12]	95.3 / 97.9 / 91.5	93.4	97.0 / 47.6 / 51.5	24.7 / 35.7 / 15.2 / 34.7	94.9 / 65.4 / 25.2
	UniAD \dagger [52]	86.9 / 93.9 / 86.0	82.0	97.3 / 46.6 / 52.4	22.2 / 43.0 / 13.6 / 35.5	88.9 / 65.4 / 26.3
	DeSTSeg* [60]	92.1 / 96.1 / 89.5	47.7	88.1 / 35.2 / 38.5	21.6 / 13.0 / 12.3 / 23.8	92.6 / 53.9 / 15.6
	SimpleNet* [32]	88.4 / 93.0 / 83.3	85.1	93.0 / 39.1 / 45.4	19.8 / 30.8 / 11.9 / 29.4	88.2 / 59.2 / 20.8
pipe_fryum	DiAD [16]	89.8 / 95.0 / 87.2	81.3	97.6 / 58.6 / 60.1	11.3 / 54.4 / 6.1 / 10.1	90.7 / 72.1 / 23.9
	InvAD-lite	96.2 / 98.3 / 92.7	91.7	96.9 / 47.5 / 52.0	24.8 / 23.3 / 15.5 / 35.1	95.7 / 65.5 / 21.2
	InvAD	96.0 / 98.2 / 92.3	91.8	97.1 / 48.4 / 52.5	26.4 / 26.9 / 16.6 / 35.6	95.5 / 66.0 / 23.3
	DRÆM* [55]	82.8 / 91.2 / 84.0	61.9	91.1 / 38.2 / 39.7	13.2 / 7.4 / 7.2 / 24.8	86.0 / 56.3 / 9.3
	RD* [12]	97.9 / 98.9 / 96.5	95.4	99.1 / 56.8 / 58.8	32.5 / 44.4 / 21.0 / 41.7	97.8 / 71.6 / 32.6
	UniAD \dagger [52]	95.3 / 97.6 / 92.9	93.0	99.1 / 53.4 / 58.6	28.6 / 49.3 / 18.3 / 41.5	95.3 / 70.4 / 32.1
	DeSTSeg* [60]	94.1 / 97.1 / 91.9	45.9	98.9 / 78.8 / 72.7	43.4 / 53.1 / 28.9 / 47.1	94.4 / 83.5 / 41.8
SimpleNet* [32]	90.8 / 95.5 / 88.6	83.0	98.5 / 65.6 / 63.4	33.7 / 52.4 / 22.1 / 46.4	91.6 / 75.8 / 36.1	
	DiAD [16]	96.2 / 98.1 / 93.7	89.9	99.4 / 72.7 / 69.9	33.8 / 50.7 / 21.9 / 41.0	96.0 / 80.7 / 35.5
	InvAD-lite	98.7 / 99.3 / 96.0	94.4	99.0 / 55.6 / 57.3	33.9 / 41.4 / 22.0 / 40.1	98.0 / 70.6 / 32.4
	InvAD	99.4 / 99.7 / 98.0	94.8	99.4 / 67.4 / 66.3	39.8 / 44.5 / 27.1 / 49.6	99.0 / 77.7 / 37.1

Table A9: **Quantitative results for each class on MVTec 3D AD dataset.** These are respectively the image-level mAU-ROC/mAP/m F_1 -max, region-level **mAU-PRO**, pixel-level mAU-ROC/mAP/m F_1 -max, the proposed pixel-level m F_1 $_{.8}^2$ /mAcc $_{.8}^2$ /mIoU $_{.8}^2$ /**mIoU-max**, and averaged **mAD I** /**mAD P** /**mAD $_{.8}^2$** .

	Method	mAU-ROC/mAP/m F_1 -max	mAU-PRO	mAU-ROC/mAP/m F_1 -max	m F_1 $_{.8}^2$ /mAcc $_{.8}^2$ /mIoU $_{.8}^2$ / mIoU-max	mADI / mADP / mAD$_{.8}^2$
bagel	RD* [12]	82.5 / 95.4 / 89.6	91.3	98.6 / 39.0 / 45.1	18.9 / 65.4 / 11.3 / 29.1	89.2 / 60.9 / 31.9
	UniAD \dagger [52]	82.7 / 95.8 / 89.3	84.4	97.6 / 30.4 / 35.8	13.0 / 51.4 / 7.4 / 21.8	89.3 / 54.6 / 23.9
	SimpleNet* [32]	76.2 / 93.3 / 89.3	70.4	93.2 / 23.6 / 30.9	12.6 / 55.3 / 7.1 / 18.3	86.3 / 49.2 / 25.0
	DiAD [16]	100. / 100. / 100.	93.8	98.5 / 49.6 / 54.2	4.6 / 53.2 / 2.4 / 5.3	100. / 67.4 / 20.1
	InvAD-lite	90.9 / 97.6 / 93.0	93.6	98.8 / 43.0 / 46.6	21.1 / 68.4 / 12.8 / 30.4	93.8 / 62.8 / 34.1
	InvAD	93.5 / 98.3 / 93.8	94.7	99.1 / 44.9 / 48.7	24.0 / 62.2 / 14.6 / 32.2	95.2 / 64.2 / 33.6
cable_gland	RD* [12]	90.1 / 97.5 / 92.6	98.2	99.4 / 37.9 / 43.2	18.6 / 63.9 / 11.0 / 27.5	93.4 / 60.2 / 31.2
	UniAD \dagger [52]	89.8 / 97.2 / 93.9	96.3	98.9 / 26.4 / 34.8	11.7 / 47.5 / 6.6 / 21.1	93.6 / 53.4 / 21.9
	SimpleNet* [32]	70.3 / 91.0 / 90.2	86.8	95.2 / 14.4 / 23.1	9.1 / 68.2 / 4.9 / 13.0	83.8 / 44.2 / 27.4
	DiAD [16]	68.1 / 91.0 / 92.3	94.5	98.4 / 25.2 / 32.0	4.8 / 44.3 / 2.5 / 5.2	83.8 / 51.9 / 17.2
	InvAD-lite	94.4 / 98.7 / 95.4	98.5	99.4 / 41.1 / 46.8	23.6 / 54.0 / 14.3 / 30.5	96.2 / 62.4 / 30.6
	InvAD	97.3 / 99.3 / 96.7	98.8	99.6 / 41.5 / 47.9	25.6 / 49.9 / 15.5 / 31.5	97.8 / 63.0 / 30.3
carrot	RD* [12]	87.3 / 96.7 / 93.2	97.2	99.4 / 27.5 / 33.7	15.5 / 47.8 / 8.8 / 20.2	92.4 / 53.5 / 24.0
	UniAD \dagger [52]	76.8 / 93.8 / 92.5	93.4	98.0 / 12.2 / 19.3	9.4 / 36.5 / 5.1 / 10.7	87.7 / 43.2 / 17.0
	SimpleNet* [32]	71.4 / 92.6 / 91.2	84.4	96.4 / 13.8 / 21.2	10.1 / 55.0 / 5.5 / 11.9	85.1 / 43.8 / 23.5
	DiAD [16]	94.4 / 99.3 / 98.0	94.6	98.6 / 20.0 / 26.9	6.0 / 41.7 / 3.1 / 5.8	97.2 / 48.5 / 16.9
	InvAD-lite	90.0 / 97.3 / 94.4	98.0	99.4 / 27.0 / 33.2	18.0 / 43.5 / 10.3 / 19.9	93.9 / 53.2 / 23.9
	InvAD	89.7 / 97.4 / 94.5	96.9	99.3 / 26.3 / 30.6	18.7 / 39.2 / 10.6 / 18.1	93.9 / 52.1 / 22.8
cookie	RD* [12]	46.0 / 77.4 / 88.0	86.6	96.6 / 27.5 / 32.9	15.5 / 66.8 / 8.7 / 19.7	70.5 / 52.3 / 30.3
	UniAD \dagger [52]	77.3 / 93.5 / 88.0	88.7	97.5 / 40.4 / 45.6	18.3 / 50.0 / 10.8 / 29.5	86.3 / 61.2 / 26.4
	SimpleNet* [32]	66.7 / 89.6 / 88.4	66.6	90.5 / 26.7 / 31.4	12.0 / 42.3 / 6.7 / 18.6	81.6 / 49.5 / 20.3
	DiAD [16]	69.4 / 78.8 / 90.9	83.5	94.3 / 14.0 / 23.8	6.8 / 53.9 / 3.6 / 5.6	79.7 / 44.0 / 21.4
	InvAD-lite	64.8 / 87.3 / 88.4	87.7	97.3 / 37.1 / 40.5	18.3 / 60.7 / 10.6 / 25.4	80.2 / 58.3 / 29.9
	InvAD	64.5 / 88.1 / 88.4	93.4	98.5 / 49.6 / 50.4	20.7 / 51.9 / 12.5 / 33.7	80.3 / 66.2 / 28.4
dowel	RD* [12]	96.7 / 98.9 / 97.6	98.8	99.7 / 47.7 / 50.8	23.5 / 47.5 / 14.5 / 34.0	97.7 / 66.1 / 28.5
	UniAD \dagger [52]	96.7 / 99.3 / 96.2	96.1	99.1 / 32.1 / 37.7	20.0 / 56.2 / 11.6 / 23.2	97.4 / 56.3 / 29.3
	SimpleNet* [32]	83.7 / 95.1 / 91.7	83.0	95.3 / 17.4 / 25.6	11.3 / 62.0 / 6.2 / 14.7	90.2 / 46.1 / 26.5
	DiAD [16]	98.0 / 99.3 / 97.3	89.6	97.2 / 31.4 / 40.1	3.9 / 29.8 / 2.0 / 4.2	98.2 / 56.2 / 11.9
	InvAD-lite	97.2 / 99.4 / 96.2	97.6	99.6 / 52.6 / 51.8	31.9 / 56.7 / 20.0 / 34.9	97.6 / 68.0 / 36.2
	InvAD	99.0 / 99.8 / 99.0	98.2	99.7 / 50.8 / 49.5	31.8 / 50.5 / 19.7 / 32.9	99.3 / 66.7 / 34.0
foam	RD* [12]	74.3 / 92.9 / 90.6	79.9	94.2 / 15.0 / 26.4	12.3 / 31.5 / 6.8 / 15.2	85.9 / 45.2 / 16.9
	UniAD \dagger [52]	70.5 / 92.4 / 88.9	55.8	82.2 / 6.8 / 18.9	9.3 / 20.5 / 5.0 / 10.4	83.9 / 36.0 / 11.6
	SimpleNet* [32]	77.4 / 94.2 / 89.7	66.7	87.8 / 15.7 / 26.7	12.1 / 22.5 / 6.7 / 15.4	87.1 / 43.4 / 13.8
	DiAD [16]	100. / 100. / 100.	69.1	89.8 / 9.6 / 23.5	1.8 / 54.9 / 0.9 / 2.7	100. / 41.0 / 19.2
	InvAD-lite	83.6 / 95.7 / 90.4	81.6	94.8 / 24.3 / 32.3	20.4 / 39.1 / 11.7 / 19.3	89.9 / 50.5 / 23.7
	InvAD	77.3 / 93.5 / 90.8	78.4	93.8 / 18.3 / 30.8	16.2 / 35.5 / 9.1 / 18.2	87.2 / 47.6 / 20.3
peach	RD* [12]	64.3 / 84.8 / 90.6	93.2	98.5 / 15.5 / 22.7	9.7 / 55.3 / 5.2 / 12.8	79.9 / 45.6 / 23.4
	UniAD \dagger [52]	70.0 / 91.0 / 90.5	90.4	97.4 / 11.7 / 17.9	7.8 / 61.8 / 4.1 / 9.9	83.8 / 42.3 / 24.6
	SimpleNet* [32]	62.0 / 86.9 / 89.7	74.8	92.9 / 8.1 / 15.0	6.6 / 47.6 / 3.5 / 8.1	79.5 / 38.7 / 19.2
	DiAD [16]	58.0 / 91.3 / 94.3	94.2	98.4 / 27.6 / 31.3	4.6 / 60.7 / 2.4 / 4.5	81.2 / 52.5 / 22.6
	InvAD-lite	86.8 / 96.1 / 94.1	96.5	99.2 / 40.6 / 43.3	18.9 / 62.7 / 11.1 / 27.6	92.3 / 61.0 / 30.9
	InvAD	88.8 / 96.9 / 92.6	96.2	99.2 / 39.1 / 43.6	19.6 / 63.4 / 11.6 / 27.9	92.8 / 60.6 / 31.5
potato	RD* [12]	62.5 / 88.5 / 90.5	95.9	99.1 / 14.9 / 22.5	10.4 / 61.6 / 5.7 / 12.7	80.5 / 45.5 / 25.9
	UniAD \dagger [52]	51.6 / 81.8 / 89.3	91.1	97.6 / 5.1 / 8.9	3.3 / 32.7 / 1.7 / 4.7	74.2 / 37.2 / 12.6
	SimpleNet* [32]	56.7 / 82.2 / 89.8	72.8	91.0 / 4.3 / 10.9	4.8 / 56.8 / 2.5 / 5.8	76.2 / 35.4 / 21.4
	DiAD [16]	76.3 / 94.3 / 95.0	93.9	98.0 / 8.6 / 17.8	6.2 / 66.1 / 3.3 / 7.8	88.5 / 41.5 / 25.2
	InvAD-lite	63.4 / 86.0 / 92.0	95.5	99.1 / 15.6 / 20.9	11.5 / 61.5 / 6.2 / 11.7	80.5 / 45.2 / 26.4
	InvAD	67.7 / 90.5 / 90.2	96.0	99.1 / 18.9 / 25.2	13.8 / 63.8 / 7.6 / 14.4	82.8 / 47.7 / 28.4
rope	RD* [12]	96.3 / 98.5 / 93.2	97.9	99.6 / 50.3 / 55.9	22.9 / 37.5 / 14.4 / 38.8	96.0 / 68.6 / 24.9
	UniAD \dagger [52]	97.4 / 99.0 / 95.5	94.3	99.0 / 34.5 / 40.7	23.7 / 50.7 / 14.1 / 25.5	97.3 / 58.1 / 29.5
	SimpleNet* [32]	95.6 / 98.4 / 94.7	92.8	99.3 / 51.1 / 52.9	25.8 / 67.4 / 16.2 / 36.0	96.2 / 67.8 / 36.5
	DiAD [16]	89.2 / 95.4 / 91.9	96.5	99.3 / 61.0 / 59.9	7.5 / 56.3 / 3.9 / 7.5	92.2 / 73.4 / 22.6
	InvAD-lite	96.1 / 98.5 / 95.5	95.7	99.4 / 50.0 / 51.8	29.4 / 52.4 / 18.4 / 35.0	96.7 / 67.1 / 33.4
	InvAD	95.6 / 98.3 / 93.3	96.7	99.6 / 56.1 / 57.3	29.4 / 42.0 / 18.9 / 40.2	95.7 / 71.0 / 30.1
tire	RD* [12]	79.2 / 93.0 / 88.4	96.4	99.2 / 23.2 / 31.1	13.2 / 53.4 / 7.4 / 18.4	86.9 / 51.2 / 24.7
	UniAD \dagger [52]	75.7 / 90.7 / 89.7	90.6	98.0 / 11.9 / 20.3	5.7 / 28.9 / 3.0 / 11.3	85.4 / 43.4 / 12.5
	SimpleNet* [32]	65.3 / 86.8 / 87.9	77.9	93.8 / 8.1 / 15.3	5.8 / 50.4 / 3.1 / 8.3	80.0 / 39.1 / 19.8
	DiAD [16]	92.7 / 98.9 / 95.8	68.8	91.8 / 5.9 / 13.7	3.9 / 52.5 / 2.0 / 5.1	95.8 / 37.1 / 19.5
	InvAD-lite	85.7 / 95.6 / 90.2	96.4	99.3 / 40.9 / 46.7	22.9 / 54.3 / 14.0 / 30.5	90.5 / 62.3 / 30.4
	InvAD	87.8 / 96.2 / 92.4	97.6	99.6 / 32.3 / 40.9	20.4 / 46.3 / 11.9 / 25.7	92.1 / 57.6 / 26.2

Table A10: **Quantitative results for each class on Uni-Medical dataset.** These are respectively the image-level mAU-ROC/mAP/m F_1 -max, region-level **mAU-PRO**, pixel-level mAU-ROC/mAP/m F_1 -max, the proposed pixel-level m $F_{1.8}^2$ /mAcc $_{.8}^2$ /mIoU $_{.8}^2$ /**mIoU-max**, and averaged **mAD I** /**mAD P** /**mAD $_{.8}^2$** .

	Method	mAU-ROC/mAP/m F_1 -max	mAU-PRO	mAU-ROC/mAP/m F_1 -max	m $F_{1.8}^2$ /mAcc $_{.8}^2$ /mIoU $_{.8}^2$ /mIoU-max	mADI / mADP / mAD$_{.8}^2$
brain	RD* [12]	82.4 / 94.4 / 91.5	82.6	96.5 / 45.9 / 49.2	18.6 / 44.2 / 11.2 / 32.6	89.4 / 63.9 / 24.7
	UniAD \dagger [52]	89.9 / 97.5 / 92.6	82.4	97.4 / 55.7 / 55.7	18.2 / 45.5 / 11.2 / 38.6	93.3 / 69.6 / 25.0
	SimpleNet* [32]	82.3 / 95.6 / 90.9	73.0	94.8 / 42.1 / 42.4	13.7 / 33.9 / 8.1 / 26.9	89.6 / 59.8 / 18.6
	DiAD [16]	93.2 / 98.3 / 95.0	80.3	95.4 / 42.9 / 36.7	22.5 / 55.1 / 12.7 / 27.3	95.5 / 58.3 / 30.1
	InvAD-lite	86.8 / 96.3 / 92.0	82.6	96.6 / 47.4 / 50.1	24.2 / 49.6 / 14.8 / 33.5	91.7 / 64.7 / 29.5
liver	InvAD	90.5 / 97.6 / 93.1	87.2	98.1 / 64.0 / 61.7	28.3 / 54.4 / 18.3 / 44.6	93.7 / 74.6 / 33.7
	RD* [12]	55.1 / 46.3 / 64.1	89.9	96.6 / 5.7 / 10.3	6.4 / 43.6 / 3.4 / 5.4	55.2 / 37.5 / 17.8
	UniAD \dagger [52]	61.0 / 48.8 / 63.2	92.7	97.1 / 7.8 / 13.7	5.6 / 40.4 / 2.9 / 7.4	57.7 / 39.5 / 16.3
	SimpleNet* [32]	55.8 / 47.6 / 60.9	86.3	97.4 / 13.2 / 20.1	8.5 / 55.7 / 4.6 / 11.2	54.8 / 43.6 / 22.9
	DiAD [16]	70.6 / 64.7 / 65.6	91.4	97.1 / 13.7 / 7.3	7.1 / 26.7 / 3.3 / 7.3	67.0 / 39.4 / 12.3
retinal	InvAD-lite	60.0 / 48.6 / 63.7	89.2	96.4 / 5.7 / 10.1	6.6 / 39.2 / 3.5 / 5.3	57.4 / 37.4 / 16.4
	InvAD	64.8 / 52.5 / 66.6	93.3	97.2 / 8.7 / 15.8	9.1 / 45.9 / 4.8 / 8.6	61.3 / 40.6 / 19.9
	RD* [12]	89.2 / 86.7 / 78.5	86.5	96.4 / 64.7 / 60.9	24.0 / 41.9 / 15.4 / 43.8	84.8 / 74.0 / 27.1
	UniAD \dagger [52]	84.6 / 79.4 / 73.9	79.9	94.8 / 49.3 / 51.3	16.2 / 27.4 / 10.0 / 34.5	79.3 / 65.1 / 17.9
	SimpleNet* [32]	88.8 / 87.6 / 78.6	82.1	95.5 / 59.5 / 56.3	22.6 / 49.8 / 14.2 / 39.2	85.0 / 70.4 / 28.9
skin	DiAD [16]	91.6 / 90.7 / 83.0	84.4	95.3 / 57.5 / 62.8	24.5 / 30.9 / 15.2 / 40.4	88.4 / 71.9 / 23.5
	InvAD-lite	91.7 / 89.9 / 81.7	84.7	96.2 / 67.2 / 61.1	23.9 / 32.8 / 15.4 / 44.0	87.8 / 74.8 / 24.0
	InvAD	91.4 / 88.7 / 82.0	88.4	97.0 / 69.8 / 63.7	27.9 / 35.2 / 18.4 / 46.8	87.4 / 76.8 / 27.2

Table A11: **Quantitative results for each class on Real-IAD dataset.** These are respectively the image-level mAU-ROC/mAP/m F_1 -max, region-level **mAU-PRO**, pixel-level mAU-ROC/mAP/m F_1 -max, the proposed pixel-level m $F_{1.8}^2$ /mAcc $_{.8}^2$ /mIoU $_{.8}^2$ /mIoU-max, and averaged **mAD I** /**mAD P** /**mAD S** . Part I.

	Method	mAU-ROC/mAP/m F_1 -max	mAU-PRO	mAU-ROC/mAP/m F_1 -max	m $F_{1.8}^2$ /mAcc $_{.8}^2$ /mIoU $_{.8}^2$ /mIoU-max	mADI / mADP / mADS
audiojack	RD* [12]	76.2 / 63.2 / 60.8	79.6	96.6 / 12.8 / 22.1	7.0 / 62.9 / 3.8 / 12.2	66.7 / 43.8 / 24.6
	UniAD \dagger [52]	82.0 / 76.7 / 65.5	84.0	97.6 / 20.5 / 31.2	11.7 / 44.6 / 6.6 / 18.5	74.7 / 49.8 / 21.0
	SimpleNet* [32]	58.4 / 44.2 / 50.9	38.0	74.4 / 0.9 / 4.8	1.3 / 45.0 / 0.7 / 2.5	51.2 / 26.7 / 15.7
	DiAD [16]	76.5 / 54.3 / 65.7	63.3	91.6 / 1.0 / 3.9	1.7 / 41.0 / 0.9 / 2.0	65.5 / 32.2 / 14.5
	InvAD-lite	84.2 / 78.8 / 67.9	86.7	98.1 / 31.6 / 41.0	17.2 / 52.0 / 10.1 / 25.8	77.0 / 56.9 / 26.4
bottle	InvAD	84.4 / 79.5 / 67.7	88.8	98.4 / 32.1 / 42.4	19.8 / 50.7 / 11.8 / 26.9	77.2 / 57.6 / 27.4
	RD* [12]	89.5 / 86.3 / 81.0	95.7	99.5 / 18.9 / 29.9	11.8 / 38.5 / 6.6 / 17.6	85.6 / 49.4 / 19.0
	UniAD \dagger [52]	92.0 / 91.3 / 80.7	95.5	99.5 / 21.0 / 29.9	13.2 / 35.9 / 7.4 / 17.6	88.0 / 50.1 / 18.8
	SimpleNet* [32]	54.1 / 47.6 / 60.3	45.1	85.3 / 2.3 / 5.7	1.6 / 47.7 / 0.8 / 2.9	54.0 / 31.1 / 16.7
	DiAD [16]	91.6 / 94.0 / 87.9	73.0	94.6 / 4.9 / 11.4	4.6 / 41.4 / 2.4 / 6.0	91.1 / 37.0 / 16.1
button	InvAD-lite	92.1 / 90.2 / 81.6	97.1	99.6 / 20.2 / 26.6	13.1 / 23.9 / 7.3 / 15.3	88.0 / 48.8 / 14.8
	InvAD	94.5 / 93.6 / 84.2	96.2	99.6 / 22.3 / 32.3	16.6 / 30.5 / 9.4 / 19.2	90.8 / 51.4 / 18.8
	RD* [12]	73.3 / 78.9 / 76.1	86.5	97.6 / 33.8 / 37.8	15.4 / 47.9 / 8.9 / 23.6	76.1 / 56.4 / 24.1
	UniAD \dagger [52]	73.4 / 79.8 / 75.1	78.0	96.4 / 28.5 / 35.4	10.0 / 39.2 / 5.6 / 21.5	76.1 / 53.4 / 18.3
	SimpleNet* [32]	52.5 / 60.5 / 72.4	40.5	75.9 / 3.2 / 6.6	2.7 / 40.7 / 1.4 / 3.4	61.8 / 28.6 / 14.9
battery	DiAD [16]	80.5 / 71.3 / 70.6	66.9	84.1 / 1.4 / 5.3	2.0 / 21.2 / 1.0 / 2.7	74.2 / 30.2 / 8.0
	InvAD-lite	82.3 / 87.2 / 78.8	88.4	98.5 / 50.7 / 52.5	23.7 / 38.4 / 14.7 / 35.6	82.8 / 67.2 / 25.6
	InvAD	89.3 / 91.7 / 83.5	92.0	99.1 / 55.4 / 54.9	26.9 / 37.1 / 17.1 / 37.8	88.2 / 69.8 / 27.0
end	RD* [12]	79.8 / 84.0 / 77.8	89.2	96.7 / 12.5 / 22.5	7.2 / 38.0 / 3.9 / 12.0	80.5 / 43.9 / 16.4
	UniAD \dagger [52]	80.4 / 85.9 / 77.6	85.0	95.7 / 9.2 / 17.4	6.1 / 29.8 / 3.3 / 9.5	81.3 / 40.8 / 13.1
	SimpleNet* [32]	51.6 / 60.8 / 72.9	25.7	63.1 / 0.5 / 2.8	0.9 / 37.5 / 0.4 / 1.4	61.8 / 22.1 / 12.9
	DiAD [16]	85.1 / 83.4 / 84.8	38.2	81.3 / 2.0 / 6.9	2.2 / 37.2 / 1.1 / 3.6	84.4 / 30.1 / 13.5
	InvAD-lite	79.9 / 84.4 / 78.2	90.3	97.4 / 13.4 / 20.8	9.4 / 20.8 / 5.1 / 11.6	80.8 / 43.9 / 11.8
eraser	InvAD	84.8 / 88.3 / 80.8	93.4	98.0 / 14.4 / 22.6	10.3 / 26.2 / 5.6 / 12.7	84.6 / 45.0 / 14.0
	RD* [12]	90.0 / 88.7 / 79.7	96.0	99.5 / 30.8 / 36.7	13.6 / 47.9 / 7.8 / 22.3	86.1 / 55.7 / 23.1
	UniAD \dagger [52]	89.6 / 88.0 / 79.6	94.1	99.3 / 24.7 / 31.3	11.4 / 35.5 / 6.5 / 18.5	85.7 / 51.8 / 17.8
	SimpleNet* [32]	46.4 / 39.1 / 55.8	42.8	80.6 / 2.7 / 7.1	2.4 / 38.7 / 1.2 / 3.7	47.1 / 30.1 / 14.1
	DiAD [16]	80.0 / 80.0 / 77.3	67.5	91.1 / 7.7 / 15.4	7.9 / 32.1 / 4.2 / 8.4	79.1 / 38.1 / 14.7
fire	InvAD-lite	88.9 / 87.4 / 77.8	94.7	99.3 / 28.9 / 33.8	16.3 / 38.8 / 9.3 / 20.3	84.7 / 54.0 / 21.5
	InvAD	91.7 / 90.0 / 81.0	94.9	99.4 / 28.2 / 34.2	18.0 / 42.8 / 10.3 / 20.6	87.6 / 53.9 / 23.7
	RD* [12]	78.3 / 70.1 / 64.5	87.9	98.9 / 27.7 / 35.2	13.0 / 56.7 / 7.4 / 20.9	71.0 / 53.9 / 25.7
	UniAD \dagger [52]	80.6 / 74.5 / 67.3	84.7	98.6 / 24.5 / 32.5	13.0 / 52.9 / 7.4 / 19.4	74.1 / 51.9 / 24.4
	SimpleNet* [32]	58.1 / 41.9 / 54.4	25.3	70.5 / 0.3 / 2.2	0.6 / 40.7 / 0.3 / 1.1	51.5 / 24.3 / 13.9
hood	DiAD [16]	83.3 / 81.7 / 80.5	66.7	91.8 / 3.2 / 9.2	3.3 / 33.8 / 1.7 / 4.8	81.8 / 34.7 / 12.9
	InvAD-lite	79.9 / 73.9 / 65.6	87.4	98.8 / 24.1 / 31.2	12.6 / 40.2 / 7.1 / 18.5	73.1 / 51.4 / 20.0
	InvAD	81.4 / 74.1 / 67.3	88.6	99.0 / 25.6 / 33.2	12.9 / 40.4 / 7.3 / 19.9	74.3 / 52.6 / 20.2
mint	RD* [12]	65.8 / 63.1 / 64.8	72.3	95.0 / 11.7 / 23.0	5.6 / 42.9 / 3.1 / 12.1	64.6 / 43.2 / 17.2
	UniAD \dagger [52]	66.8 / 67.6 / 64.2	62.4	94.5 / 8.5 / 20.9	4.6 / 26.7 / 2.5 / 11.7	66.2 / 41.3 / 11.3
	SimpleNet* [32]	52.4 / 50.3 / 63.7	43.3	79.9 / 0.9 / 3.6	1.0 / 43.2 / 0.5 / 1.8	55.5 / 28.1 / 14.9
	DiAD [16]	76.7 / 76.7 / 76.0	64.2	91.1 / 5.7 / 11.6	5.3 / 44.5 / 2.8 / 6.2	76.5 / 36.1 / 17.5
	InvAD-lite	71.7 / 73.0 / 65.8	79.9	97.3 / 18.2 / 28.5	12.2 / 33.6 / 6.9 / 16.6	70.2 / 48.0 / 17.6
mounts	InvAD	76.5 / 76.6 / 68.9	82.6	98.2 / 16.9 / 28.8	11.2 / 24.5 / 6.3 / 16.8	74.0 / 48.0 / 14.0
	RD* [12]	88.6 / 79.9 / 74.8	94.9	99.3 / 30.6 / 37.1	15.5 / 49.2 / 8.9 / 22.8	81.1 / 55.7 / 24.5
	UniAD \dagger [52]	86.8 / 73.6 / 76.3	95.1	99.4 / 27.4 / 32.9	13.7 / 36.0 / 7.9 / 19.7	78.9 / 53.2 / 19.2
	SimpleNet* [32]	58.7 / 48.1 / 52.4	46.1	80.5 / 2.2 / 6.8	2.1 / 34.3 / 1.1 / 3.5	53.1 / 29.8 / 12.5
	DiAD [16]	75.3 / 74.5 / 82.5	48.8	84.3 / 0.4 / 1.1	0.6 / 29.1 / 0.3 / 0.5	77.4 / 28.6 / 10.0
pcb	InvAD-lite	87.8 / 77.1 / 76.1	94.5	99.4 / 27.4 / 33.0	17.4 / 31.4 / 9.9 / 19.8	80.3 / 53.3 / 19.6
	InvAD	87.9 / 76.6 / 77.4	93.7	99.4 / 28.1 / 32.9	18.3 / 32.4 / 10.4 / 19.7	80.6 / 53.5 / 20.4
	RD* [12]	79.5 / 85.8 / 79.7	88.3	97.5 / 15.8 / 24.3	7.6 / 53.9 / 4.1 / 14.7	81.7 / 45.9 / 21.9
	UniAD \dagger [52]	80.6 / 87.8 / 79.1	81.6	97.2 / 20.6 / 31.0	7.6 / 39.8 / 4.2 / 18.4	82.5 / 49.6 / 17.2
	SimpleNet* [32]	54.5 / 66.0 / 75.5	41.3	78.0 / 1.4 / 4.3	1.4 / 49.5 / 0.7 / 2.2	65.3 / 27.9 / 17.2
phone	DiAD [16]	86.0 / 85.1 / 85.4	66.5	92.0 / 3.7 / 7.4	3.4 / 18.6 / 1.7 / 3.8	85.5 / 34.4 / 7.9
	InvAD-lite	90.7 / 94.5 / 85.5	94.4	99.4 / 49.1 / 52.1	22.0 / 41.0 / 13.8 / 35.2	90.2 / 66.9 / 25.6
	InvAD	91.9 / 95.2 / 86.9	94.6	99.4 / 48.2 / 51.6	24.4 / 47.2 / 15.2 / 34.8	91.3 / 66.4 / 28.9
	RD* [12]	87.5 / 83.3 / 77.1	94.5	77.3 / 22.6 / 31.7	13.7 / 37.8 / 7.8 / 18.9	82.6 / 43.9 / 19.8
	UniAD \dagger [52]	83.3 / 77.2 / 73.5	86.7	88.8 / 8.8 / 16.4	6.4 / 25.4 / 3.4 / 8.9	78.0 / 38.0 / 11.7
battery	SimpleNet* [32]	51.6 / 43.8 / 58.0	11.8	43.4 / 0.1 / 0.9	0.3 / 34.6 / 0.2 / 0.4	51.1 / 14.8 / 11.7
	DiAD [16]	82.3 / 77.7 / 75.9	85.4	96.8 / 5.3 / 11.4	4.6 / 29.5 / 2.4 / 6.0	78.6 / 37.8 / 12.2
	InvAD-lite	91.2 / 89.6 / 81.8	95.5	80.2 / 25.3 / 33.6	17.3 / 30.2 / 9.9 / 20.2	87.5 / 46.4 / 19.1
	InvAD	91.0 / 87.0 / 80.4	93.9	86.2 / 21.1 / 29.5	15.7 / 29.3 / 8.8 / 17.3	86.1 / 45.6 / 17.9

Table A12: **Quantitative results for each class on Real-IAD dataset.** These are respectively the image-level mAU-ROC/mAP/m F_1 -max, region-level **mAU-PRO**, pixel-level mAU-ROC/mAP/m F_1 -max, the proposed pixel-level m $F_{1.8}^2$ /mAcc $_{.8}^2$ /mIoU $_{.8}^2$ /mIoU-max, and averaged **mAD I** /**mAD P** /**mAD S** . Part II.

	Method	mAU-ROC/mAP/m F_1 -max	mAU-PRO	mAU-ROC/mAP/m F_1 -max	m $F_{1.8}^2$ /mAcc $_{.8}^2$ /mIoU $_{.8}^2$ /mIoU-max	mADI / mADP / mADS
plastic nut	RD* [12]	80.3 / 68.0 / 64.4	91.0	98.8 / 21.1 / 29.6	11.1 / 37.4 / 6.2 / 17.3	70.9 / 49.8 / 18.2
	UniAD \dagger [52]	79.3 / 69.7 / 62.5	89.3	98.4 / 22.1 / 28.1	10.9 / 30.8 / 6.1 / 16.4	70.5 / 49.5 / 15.9
	SimpleNet* [32]	59.2 / 40.3 / 51.8	41.5	77.4 / 0.6 / 3.6	0.8 / 58.1 / 0.4 / 1.8	50.4 / 27.2 / 19.8
	DiAD [16]	71.9 / 58.2 / 65.6	38.6	81.1 / 0.4 / 3.4	1.3 / 27.9 / 0.7 / 1.7	65.2 / 28.3 / 10.0
	InvAD-lite	88.1 / 80.6 / 72.5	96.4	99.5 / 30.2 / 34.3	18.9 / 35.5 / 10.9 / 20.7	80.4 / 54.7 / 21.8
plastic plug	InvAD	89.1 / 81.5 / 73.5	95.8	99.5 / 27.2 / 31.9	19.3 / 35.1 / 11.0 / 19.0	81.4 / 52.9 / 21.8
	RD* [12]	81.9 / 74.3 / 68.8	94.9	99.1 / 20.5 / 28.4	8.5 / 40.5 / 4.7 / 16.0	75.0 / 49.3 / 17.9
	UniAD \dagger [52]	81.1 / 76.7 / 67.1	88.7	98.6 / 17.7 / 26.7	9.2 / 43.2 / 5.1 / 15.4	75.0 / 47.7 / 19.2
	SimpleNet* [32]	48.2 / 38.4 / 54.6	38.8	78.6 / 0.7 / 1.9	0.6 / 46.7 / 0.3 / 0.9	47.1 / 27.1 / 15.9
	DiAD [16]	88.7 / 89.2 / 90.9	66.1	92.9 / 8.7 / 15.0	7.4 / 36.0 / 3.9 / 8.1	89.6 / 38.9 / 15.8
porcelain doll	InvAD-lite	88.2 / 84.6 / 74.7	93.4	99.2 / 26.7 / 34.1	14.6 / 38.0 / 8.3 / 20.5	82.5 / 53.3 / 20.3
	InvAD	89.0 / 82.5 / 76.4	93.0	99.0 / 22.1 / 29.9	12.6 / 38.3 / 7.0 / 17.6	82.6 / 50.3 / 19.3
	RD* [12]	86.3 / 76.3 / 71.5	95.7	99.2 / 24.8 / 34.6	12.7 / 40.0 / 7.2 / 20.9	78.0 / 52.9 / 20.0
	UniAD \dagger [52]	84.7 / 75.2 / 69.5	92.8	98.7 / 13.8 / 23.5	7.0 / 28.2 / 3.8 / 13.3	76.5 / 45.3 / 13.0
	SimpleNet* [32]	66.3 / 54.5 / 52.1	47.0	81.8 / 2.0 / 6.4	1.8 / 53.7 / 0.9 / 3.3	57.6 / 30.1 / 18.8
regulator	DiAD [16]	72.6 / 66.8 / 65.2	70.4	93.1 / 1.4 / 4.8	2.2 / 19.6 / 1.1 / 2.5	68.2 / 33.1 / 7.6
	InvAD-lite	88.7 / 82.8 / 74.6	95.6	99.3 / 32.0 / 36.7	18.9 / 31.7 / 11.0 / 22.5	82.0 / 56.0 / 20.5
	InvAD	86.6 / 76.5 / 69.6	91.9	98.6 / 21.3 / 32.0	14.6 / 31.8 / 8.3 / 19.1	77.6 / 50.6 / 18.2
	RD* [12]	66.9 / 48.8 / 47.7	88.6	98.0 / 7.8 / 16.1	4.8 / 49.4 / 2.5 / 8.2	54.5 / 40.6 / 18.9
	UniAD \dagger [52]	52.6 / 34.9 / 44.3	70.3	94.2 / 7.6 / 15.0	4.8 / 41.3 / 2.5 / 8.1	43.9 / 38.9 / 16.2
rolled strip base	SimpleNet* [32]	50.5 / 29.0 / 43.9	38.1	76.6 / 0.1 / 0.6	0.2 / 61.8 / 0.1 / 0.3	41.1 / 25.8 / 20.7
	DiAD [16]	72.1 / 71.4 / 78.2	44.4	84.2 / 0.4 / 1.5	0.6 / 35.9 / 0.3 / 0.7	73.9 / 28.7 / 12.3
	InvAD-lite	75.7 / 66.7 / 57.7	92.3	98.7 / 18.7 / 29.9	10.5 / 22.2 / 5.9 / 17.6	66.7 / 49.1 / 12.9
	InvAD	84.6 / 78.1 / 67.8	95.8	99.5 / 24.2 / 33.2	14.8 / 30.0 / 8.5 / 19.9	76.8 / 52.3 / 17.8
	RD* [12]	97.5 / 98.7 / 94.7	98.4	99.7 / 31.4 / 39.9	14.2 / 40.8 / 8.3 / 24.2	97.0 / 57.0 / 21.1
sim card set	UniAD \dagger [52]	98.6 / 99.3 / 96.0	97.8	99.6 / 21.5 / 32.4	9.6 / 24.5 / 5.4 / 19.4	98.0 / 51.2 / 13.2
	SimpleNet* [32]	59.0 / 75.7 / 79.8	52.1	80.5 / 1.7 / 5.1	2.0 / 27.4 / 1.0 / 2.6	71.5 / 29.1 / 10.1
	DiAD [16]	68.4 / 55.9 / 56.8	63.4	87.7 / 0.6 / 3.2	1.3 / 36.7 / 0.6 / 1.6	60.4 / 30.5 / 12.9
	InvAD-lite	98.0 / 99.0 / 95.2	98.9	99.8 / 31.8 / 41.1	18.3 / 33.5 / 10.8 / 25.9	97.4 / 57.6 / 20.9
	InvAD	99.3 / 99.6 / 97.5	98.8	99.8 / 32.2 / 42.0	16.4 / 29.5 / 9.7 / 26.6	98.8 / 58.0 / 18.5
switch	RD* [12]	91.6 / 91.8 / 84.8	89.5	98.5 / 40.2 / 44.2	18.4 / 51.6 / 11.0 / 28.4	89.4 / 61.0 / 27.0
	UniAD \dagger [52]	90.7 / 91.2 / 83.5	84.3	97.8 / 33.6 / 39.9	14.3 / 31.3 / 8.4 / 24.9	88.5 / 57.1 / 18.0
	SimpleNet* [32]	63.1 / 69.7 / 70.8	30.8	71.0 / 6.8 / 14.3	4.2 / 31.5 / 2.2 / 7.7	67.9 / 30.7 / 12.6
	DiAD [16]	72.6 / 53.7 / 61.5	60.4	89.9 / 1.7 / 5.8	2.3 / 40.6 / 1.2 / 3.0	62.6 / 32.5 / 14.7
	InvAD-lite	94.2 / 94.7 / 87.9	88.7	98.6 / 46.3 / 47.0	24.3 / 46.1 / 14.8 / 30.7	92.3 / 64.0 / 28.4
tape	InvAD	93.9 / 94.1 / 87.7	83.1	97.9 / 35.4 / 41.5	19.9 / 43.0 / 11.8 / 26.2	91.9 / 58.3 / 24.9
	RD* [12]	84.3 / 87.2 / 77.9	90.9	94.4 / 18.9 / 26.6	11.7 / 34.2 / 6.5 / 15.8	83.1 / 46.6 / 17.5
	UniAD \dagger [52]	85.5 / 88.9 / 78.5	91.2	99.0 / 55.6 / 57.9	19.9 / 46.6 / 12.8 / 40.8	84.3 / 70.8 / 26.4
	SimpleNet* [32]	62.2 / 66.8 / 68.6	44.2	71.7 / 3.7 / 9.3	3.0 / 37.5 / 1.6 / 4.9	65.9 / 28.2 / 14.0
	DiAD [16]	73.4 / 49.4 / 61.2	64.2	90.5 / 1.4 / 5.3	1.9 / 49.4 / 1.0 / 2.7	61.3 / 32.4 / 17.4
toothbrush terminalblock	InvAD-lite	92.9 / 94.7 / 87.2	94.9	99.0 / 41.0 / 46.4	21.7 / 30.0 / 13.1 / 30.2	91.6 / 62.1 / 21.6
	InvAD	95.7 / 96.7 / 91.1	95.7	98.9 / 42.4 / 49.7	24.3 / 32.6 / 14.9 / 33.1	94.5 / 63.7 / 23.9
	RD* [12]	96.0 / 95.1 / 87.6	98.4	99.7 / 42.4 / 47.8	21.6 / 58.1 / 13.1 / 30.4	92.9 / 63.3 / 30.9
	UniAD \dagger [52]	97.1 / 96.1 / 89.0	97.3	99.7 / 31.4 / 37.8	15.7 / 42.2 / 9.2 / 23.3	94.1 / 56.3 / 22.4
	SimpleNet* [32]	49.9 / 41.1 / 54.5	41.4	77.5 / 1.2 / 3.9	1.3 / 37.6 / 0.7 / 2.0	48.5 / 27.5 / 13.2
tape	DiAD [16]	73.9 / 57.8 / 66.1	47.3	81.7 / 0.4 / 2.7	0.8 / 33.4 / 0.4 / 1.3	65.9 / 28.2 / 11.5
	InvAD-lite	97.5 / 96.6 / 89.9	98.3	99.7 / 42.0 / 46.3	22.4 / 39.7 / 13.5 / 30.1	94.7 / 62.7 / 25.2
	InvAD	97.5 / 96.3 / 90.8	97.8	99.7 / 36.9 / 42.9	21.0 / 40.5 / 12.5 / 27.3	94.9 / 59.8 / 24.7
	RD* [12]	89.4 / 89.7 / 83.1	97.6	99.5 / 27.4 / 35.8	12.8 / 45.8 / 7.3 / 21.6	87.4 / 54.2 / 22.0
	UniAD \dagger [52]	87.4 / 89.4 / 80.9	94.1	99.2 / 23.1 / 31.1	11.1 / 42.2 / 6.3 / 18.4	85.9 / 51.1 / 19.9
switch	SimpleNet* [32]	59.8 / 64.7 / 68.8	54.8	87.0 / 0.8 / 3.6	1.1 / 51.7 / 0.6 / 1.8	64.4 / 30.5 / 17.8
	DiAD [16]	62.1 / 36.4 / 47.8	38.5	75.5 / 0.1 / 1.1	0.4 / 13.3 / 0.2 / 0.5	48.8 / 25.6 / 4.6
	InvAD-lite	96.6 / 97.3 / 90.7	98.7	99.8 / 34.5 / 37.9	20.9 / 40.7 / 12.2 / 23.4	94.9 / 57.4 / 24.6
	InvAD	97.1 / 97.8 / 91.9	98.4	99.8 / 34.6 / 37.6	22.1 / 40.3 / 12.9 / 23.2	95.6 / 57.3 / 25.1
	RD* [12]	82.0 / 83.8 / 77.2	88.7	96.9 / 26.1 / 34.2	14.2 / 46.6 / 8.1 / 20.8	81.0 / 52.4 / 23.0
toothbrush terminalblock	UniAD \dagger [52]	81.4 / 82.6 / 78.0	85.8	96.1 / 20.0 / 29.7	11.5 / 40.7 / 6.4 / 17.4	80.7 / 48.6 / 19.5
	SimpleNet* [32]	65.9 / 70.0 / 70.1	52.6	84.7 / 7.2 / 14.8	5.0 / 40.8 / 2.6 / 8.0	68.7 / 35.6 / 16.1
	DiAD [16]	91.2 / 93.7 / 90.9	54.5	82.0 / 1.9 / 6.6	2.4 / 14.3 / 1.2 / 3.4	91.9 / 30.1 / 6.0
	InvAD-lite	86.8 / 88.5 / 80.4	90.8	97.4 / 29.2 / 37.0	18.6 / 41.7 / 10.8 / 22.7	85.2 / 54.5 / 23.7
	InvAD	88.3 / 89.8 / 81.7	90.6	97.5 / 28.7 / 36.9	17.9 / 36.1 / 10.4 / 22.6	86.6 / 54.4 / 21.5

Table A13: **Quantitative results for each class on Real-IAD dataset.** These are respectively the image-level mAU-ROC/mAP/m F_1 -max, region-level **mAU-PRO**, pixel-level mAU-ROC/mAP/m F_1 -max, the proposed pixel-level m $F_{1.8}^2$ /mAcc $_{.8}^2$ /mIoU $_{.8}^2$ /mIoU-max, and averaged **mAD I** /**mAD P** /**mAD S** . Part III.

	Method	mAU-ROC/mAP/m F_1 -max	mAU-PRO	mAU-ROC/mAP/m F_1 -max	m $F_{1.8}^2$ /mAcc $_{.8}^2$ /mIoU $_{.8}^2$ /mIoU-max	mADI / mADP / mADS
toy	RD* [12]	69.4 / 74.2 / 75.9	82.3	95.2 / 5.1 / 12.8	3.2 / 33.2 / 1.6 / 6.2	73.2 / 37.7 / 12.7
	UniAD \dagger [52]	67.9 / 74.6 / 74.4	70.2	93.6 / 4.4 / 10.7	2.8 / 27.1 / 1.5 / 5.6	72.3 / 36.2 / 10.5
	SimpleNet* [32]	57.8 / 64.4 / 73.4	25.0	67.7 / 0.1 / 0.4	0.2 / 23.4 / 0.1 / 0.2	65.2 / 22.7 / 7.9
	DiAD [16]	66.2 / 57.3 / 59.8	50.3	82.1 / 1.1 / 4.2	1.3 / 58.5 / 0.7 / 2.1	61.1 / 29.1 / 20.2
	InvAD-lite	84.2 / 88.8 / 80.1	89.1	96.7 / 18.7 / 29.3	12.2 / 30.0 / 6.8 / 17.2	84.4 / 48.2 / 16.3
	InvAD	85.7 / 89.0 / 82.4	91.0	98.1 / 15.6 / 24.8	8.3 / 15.4 / 4.6 / 14.2	85.7 / 46.2 / 9.4
toy brick	RD* [12]	63.6 / 56.1 / 59.0	75.3	96.4 / 16.0 / 24.6	7.6 / 48.7 / 4.1 / 13.1	59.6 / 45.7 / 20.1
	UniAD \dagger [52]	78.6 / 74.4 / 67.4	81.5	97.7 / 21.3 / 29.4	8.7 / 34.4 / 4.9 / 17.2	73.5 / 49.5 / 16.0
	SimpleNet* [32]	58.3 / 49.7 / 58.2	56.3	86.5 / 5.2 / 11.1	3.9 / 44.3 / 2.1 / 5.9	55.4 / 34.3 / 16.8
	DiAD [16]	68.4 / 45.3 / 55.9	66.4	93.5 / 3.1 / 8.1	2.8 / 52.4 / 1.4 / 4.2	56.5 / 34.9 / 18.9
	InvAD-lite	69.3 / 61.9 / 60.8	78.1	96.5 / 15.9 / 23.9	8.6 / 46.6 / 4.7 / 13.6	64.0 / 45.4 / 20.0
	InvAD	72.4 / 65.5 / 63.3	80.2	97.3 / 23.4 / 30.6	10.4 / 35.0 / 5.8 / 18.1	67.1 / 50.4 / 17.1
transistor	RD* [12]	91.0 / 94.0 / 85.1	95.1	99.1 / 29.6 / 35.5	14.6 / 53.4 / 8.4 / 21.9	90.0 / 54.7 / 25.5
	UniAD \dagger [52]	94.2 / 96.2 / 89.4	94.2	99.0 / 26.6 / 33.6	12.4 / 43.0 / 7.1 / 20.2	93.3 / 53.1 / 20.8
	SimpleNet* [32]	62.2 / 69.2 / 72.1	35.3	71.7 / 5.1 / 11.3	3.7 / 45.0 / 1.9 / 6.0	67.8 / 29.4 / 16.9
	DiAD [16]	73.1 / 63.1 / 62.7	58.1	88.6 / 7.2 / 15.3	5.6 / 33.9 / 3.0 / 8.3	66.3 / 37.0 / 14.2
	InvAD-lite	96.2 / 97.3 / 92.2	96.9	99.5 / 40.6 / 42.1	19.1 / 37.9 / 11.3 / 26.7	95.2 / 60.7 / 22.8
	InvAD	97.3 / 98.1 / 93.6	97.0	99.5 / 35.1 / 37.9	20.9 / 43.2 / 12.2 / 23.4	96.3 / 57.5 / 25.4
u block	RD* [12]	89.5 / 85.0 / 74.2	96.9	99.6 / 40.5 / 45.2	17.7 / 53.2 / 10.5 / 29.1	82.9 / 61.8 / 27.1
	UniAD \dagger [52]	88.1 / 83.1 / 73.5	94.7	99.3 / 22.8 / 30.1	9.9 / 25.6 / 5.6 / 17.7	81.6 / 50.7 / 13.7
	SimpleNet* [32]	62.4 / 48.4 / 51.8	34.0	76.2 / 4.8 / 12.2	3.8 / 30.7 / 2.0 / 6.5	54.2 / 31.1 / 12.2
	DiAD [16]	75.2 / 68.4 / 67.9	54.2	88.8 / 1.6 / 5.4	2.0 / 56.0 / 1.0 / 2.8	70.5 / 31.9 / 19.6
	InvAD-lite	89.9 / 85.4 / 75.5	96.4	99.6 / 33.8 / 42.0	20.0 / 36.3 / 11.7 / 26.6	83.6 / 58.5 / 22.7
	InvAD	92.3 / 88.5 / 79.3	96.5	99.6 / 30.9 / 39.6	17.6 / 32.7 / 10.2 / 24.7	86.7 / 56.7 / 20.2
usb	RD* [12]	84.9 / 84.3 / 75.1	91.0	98.1 / 26.4 / 35.2	11.8 / 41.9 / 6.8 / 21.1	81.4 / 53.2 / 20.2
	UniAD \dagger [52]	80.5 / 81.4 / 71.0	85.9	98.1 / 19.9 / 29.7	8.0 / 30.5 / 4.5 / 17.4	77.6 / 49.2 / 14.3
	SimpleNet* [32]	57.0 / 55.3 / 62.9	52.4	81.1 / 1.5 / 4.9	1.2 / 30.8 / 0.6 / 2.5	58.4 / 29.2 / 10.9
	DiAD [16]	58.9 / 37.4 / 45.7	28.0	78.0 / 1.0 / 3.1	1.3 / 39.7 / 0.7 / 1.6	47.3 / 27.4 / 13.9
	InvAD-lite	93.1 / 92.8 / 85.5	96.6	99.5 / 37.7 / 43.6	23.9 / 46.9 / 14.3 / 27.9	90.5 / 60.3 / 28.4
	InvAD	93.6 / 92.8 / 86.3	97.1	99.5 / 36.7 / 42.7	19.0 / 32.2 / 11.4 / 27.1	90.9 / 59.6 / 20.9
usb adaptor	RD* [12]	71.1 / 61.4 / 62.2	73.1	94.5 / 9.8 / 17.9	7.6 / 35.3 / 4.1 / 10.3	64.9 / 40.7 / 15.7
	UniAD \dagger [52]	76.6 / 71.8 / 64.2	78.9	96.4 / 10.9 / 19.7	7.6 / 27.5 / 4.1 / 10.9	70.9 / 42.3 / 13.1
	SimpleNet* [32]	47.5 / 38.4 / 56.5	28.9	67.9 / 0.2 / 1.3	0.4 / 46.8 / 0.2 / 0.6	47.5 / 23.1 / 15.8
	DiAD [16]	76.9 / 60.2 / 67.2	75.5	94.0 / 2.3 / 6.6	2.7 / 39.0 / 1.4 / 3.4	68.1 / 34.3 / 14.3
	InvAD-lite	79.5 / 73.3 / 67.3	80.1	97.1 / 16.1 / 24.5	12.7 / 30.2 / 7.0 / 13.9	73.4 / 45.9 / 16.6
	InvAD	79.7 / 73.1 / 66.3	77.0	96.2 / 15.0 / 23.6	10.8 / 27.4 / 5.9 / 13.4	73.0 / 44.9 / 14.7
vepill	RD* [12]	85.1 / 80.3 / 72.4	88.7	98.3 / 43.1 / 48.6	13.6 / 37.8 / 8.2 / 32.1	79.3 / 63.3 / 19.9
	UniAD \dagger [52]	88.0 / 85.7 / 75.4	92.0	99.2 / 47.3 / 47.4	12.0 / 21.6 / 7.3 / 31.1	83.0 / 64.6 / 13.6
	SimpleNet* [32]	59.0 / 48.7 / 56.4	22.0	68.2 / 1.1 / 3.3	1.2 / 39.5 / 0.6 / 1.7	54.7 / 24.2 / 13.8
	DiAD [16]	64.1 / 40.4 / 56.2	60.8	90.2 / 1.3 / 5.2	1.9 / 32.8 / 1.0 / 2.7	53.6 / 32.3 / 11.9
	InvAD-lite	84.1 / 81.4 / 70.9	87.0	98.4 / 41.6 / 49.5	18.3 / 37.6 / 11.0 / 32.8	78.8 / 63.2 / 22.3
	InvAD	89.4 / 87.2 / 77.9	90.3	98.8 / 47.7 / 54.0	18.4 / 30.9 / 11.5 / 37.0	84.8 / 66.8 / 20.3
wooden beads	RD* [12]	81.2 / 78.9 / 70.9	85.7	98.0 / 27.1 / 34.7	13.6 / 57.3 / 7.8 / 21.3	77.0 / 53.3 / 26.2
	UniAD \dagger [52]	80.5 / 79.8 / 69.5	84.0	97.7 / 19.9 / 27.0	10.0 / 35.7 / 5.6 / 15.6	76.6 / 48.2 / 17.1
	SimpleNet* [32]	55.1 / 52.0 / 60.2	28.3	68.1 / 2.4 / 6.0	2.0 / 32.7 / 1.0 / 3.1	55.8 / 25.5 / 11.9
	DiAD [16]	62.1 / 56.4 / 65.9	45.6	85.0 / 1.1 / 4.7	1.8 / 39.6 / 0.9 / 2.4	61.5 / 30.3 / 14.1
	InvAD-lite	85.4 / 84.4 / 74.8	88.1	98.3 / 30.6 / 37.7	16.4 / 38.3 / 9.5 / 23.2	81.5 / 55.5 / 21.4
	InvAD	86.4 / 85.2 / 75.8	87.3	98.4 / 33.9 / 39.1	19.8 / 44.6 / 11.6 / 24.3	82.5 / 57.1 / 25.3
woodstick	RD* [12]	76.9 / 61.2 / 58.1	85.0	97.8 / 30.7 / 38.4	15.4 / 52.8 / 8.9 / 23.2	65.4 / 55.6 / 25.7
	UniAD \dagger [52]	81.2 / 73.5 / 64.4	76.4	94.7 / 40.2 / 45.9	19.5 / 39.1 / 11.8 / 29.8	73.0 / 60.3 / 23.5
	SimpleNet* [32]	58.2 / 35.6 / 45.2	32.0	76.1 / 1.4 / 6.0	1.9 / 48.1 / 1.0 / 3.1	46.3 / 27.8 / 17.0
	DiAD [16]	74.1 / 66.0 / 62.1	60.7	90.9 / 2.6 / 8.0	3.3 / 27.1 / 1.7 / 4.2	67.4 / 33.8 / 10.7
	InvAD-lite	78.5 / 65.9 / 60.3	83.1	97.6 / 36.7 / 41.6	19.9 / 49.3 / 11.9 / 26.2	68.2 / 58.6 / 27.0
	InvAD	80.8 / 67.4 / 62.2	85.5	98.0 / 37.4 / 43.3	22.4 / 50.6 / 13.4 / 27.6	70.1 / 59.6 / 28.8
zipper	RD* [12]	95.3 / 97.2 / 91.2	96.3	99.1 / 44.7 / 50.2	20.0 / 53.6 / 12.2 / 34.2	94.6 / 64.7 / 28.6
	UniAD \dagger [52]	98.1 / 98.9 / 95.5	94.7	98.3 / 32.2 / 35.5	12.7 / 28.3 / 7.3 / 21.6	97.5 / 55.3 / 16.1
	SimpleNet* [32]	77.2 / 86.7 / 77.6	55.5	89.9 / 23.3 / 31.2	13.2 / 50.6 / 7.4 / 18.5	80.5 / 48.1 / 23.7
	DiAD [16]	86.0 / 87.0 / 84.0	53.5	90.2 / 12.5 / 18.8	9.7 / 31.6 / 5.2 / 10.4	85.6 / 40.5 / 15.5
	InvAD-lite	98.9 / 99.4 / 95.8	96.7	99.2 / 55.5 / 57.9	25.0 / 42.5 / 15.8 / 40.8	98.0 / 70.9 / 27.8
	InvAD	98.7 / 99.1 / 95.9	96.1	99.1 / 48.3 / 52.4	26.7 / 52.0 / 16.6 / 35.5	97.9 / 66.6 / 31.8